International Journal of Thermofluids 21 (2024) 100484

Contents lists available at ScienceDirect

International Journal of Thermofluids

journal homepage: www.sciencedirect.com/journal/international-journal-of-thermofluids

Hydromagnetic flow of Casson nano-fluid across a stretched sheet in the presence of thermoelectric and radiation

Md. Yousuf Ali [a], Sk. Reza-E-Rabbi [b,*], Sarder Firoz Ahmmed [b], Md Nurun Nabi [c], Abul Kalam Azad [c], S.M. Muyeen [d,*]

[a] Department of Software Engineering, Daffodil International University, Dhaka 1216, Bangladesh
[b] Mathematics Discipline, Khulna University, Khulna 9208, Bangladesh
[c] School of Engineering and Technology, Central Queensland University, 120 Spencer Street, Melbourne 3000,VIC, Australia
[d] Electrical Engineering Department, Qatar University, Doha, Qatar

ARTICLE INFO

Keywords:
Thermoelectric
Radiation
Casson nano-fluid
Stretching sheet
Stream lines
Isothermal lines

ABSTRACT

This work revealed the investigation of the Casson nanofluid flow's MHD (magneto-hydrodynamic) unstable boundary layer characteristics in the simultaneous transmission of thermoelectric and radiation on a stretched sheet. On MHD Newtonian and non-Newtonian (Casson) nanofluid flows, the cumulative impact of radiation and thermoelectricity has been addressed. Thermal radiation, Casson nanofluids, and MHD are pivotal in engineering and industry, transforming applications like heat exchangers, nuclear power plants, thermal energy storage, and advanced drug delivery systems. The problem-related partial differential equations have been formulated with boundary layer approximation. The boundary layer equations have been changed into dimensionless form with the help of appropriate dimensionless variables and parameters. Finite difference techniques have been employed to get the numerical solution via the FORTRAN 6.6a programming algorithm, and the numerical solutions have been illustrated graphically with the support of Tecplot-360 software. The consequences of the numerous parameters have been investigated using a variety of figures, with the amounts of the various parameters being revised. The simultaneous effects of thermoelectric and radiation on primary velocity, secondary velocity, and temperature profiles have been presented and discussed with critical physical properties such as skin friction in addition to Nusselt number. The combined effects of thermoelectric and radiation on streamlines and isotherms have been illustrated with line and contour flood views. The most significant finding is that the collective influence of thermoelectric and thermal radiation impacts promotes the physical phenomena of non-Newtonian (Casson) fluid flow comparatively more than Newtonian fluid flow. For the purpose of creating effective procedures, forecasting flow patterns, and guaranteeing product performance in a variety of industries, it is crucial to explain the Casson fluids. This model can also aid in blood flow simulation and risk assessment for thrombosis and other cardiovascular diseases.

1. Introduction

Nowadays, many researchers are focusing on MHD Casson nano-fluids for their widespread applications, for example, photodynamic therapy, biological materials, food processing, and engineering. According to Choi [1], the type of fluid that carries nanoparticles (size 1–100 nanometers) is basically known as nano-fluid. In non-Newtonian fluids, the connection between shear stress and strain is non-linear. Within these, the Casson fluid is extraordinary (e.g., human blood, tomato sauce, jelly, honey, coal tar, etc.) at an unbounded viscosity, which pretends the non-entity shear stress rate and vice versa by Casson [2]. Actually, Casson fluids are a particular class of non-Newtonian fluids distinguished by their distinctive rheological behaviour. The connection between shear stress and shear rate in Casson fluids is nonlinear, in contrast to Newtonian fluids, which have a linear relationship. To begin flowing, they require a specific minimum shear stress, sometimes referred to as the yield stress. Casson fluids act like solids when they are below the yield stress, but when they are above it, they flow like conventional viscous fluids. The effect of thermoelectrics on MHD slip flow was researched by Abd El-Aziz et al. [3], where the flow passed a stretching sheet. Casson nanofluid flow was considered in their

* Corresponding author.
E-mail addresses: rabbi06@math.ku.ac.bd (Sk. Reza-E-Rabbi), sm.muyeen@qu.edu.qa (S.M. Muyeen).

https://doi.org/10.1016/j.ijft.2023.100484

Available online 12 October 2023

Nomenclature

Variables and Parameters

x, y	cartesian coordinates
X, Y	dimensionless cartesian coordinates
t^*	time parameter
t	dimensionless time parameter
u, v	velocity components along x- and y- directions
U, V	dimensionless velocity components along x- and y-directions
T^*	temperature
T	dimensionless temperature
C^*	concentration
C	dimensionless concentration
w	secondary velocity component perpendicular to u
W	dimensionless secondary velocity component perpendicular to u
m	hall current parameter
n	stretching rate
c_p	specific heat at constant pressure
k^*	absorption parameter
q_r	radioactive heat flux
g	acceleration due to gravity
C_f	skin-friction

Full Form

MHD	magnetohydrodynamics
EFDM	explicit finite difference method
PDE's	partial differential equations
ODE's	ordinary differential equations

Variables and Parameters

Gr	Grashof number
Gm	modified Grashof number
B_0	magnetic field
M	magnetic parameter
Pr	Prandtl number
N_r	radiation parameter
N_b	Brownian parameter
N_t	thermophoresis parameter
Le	Lewis number
Re_x	local reynolds number
Nu	Nusselt number
Sh	Sherwood number
J	Joule number

Greek symbols

α	thermal diffusivity
γ	Casson parameter
β	thermal expansion coefficient
μ_c	plastic viscosity
σ	electrical conductivity
ζ	deformation rate
ρ	fluid density
π	stress tensor
τ	ratio of effective heat capacity
P_y	yield stress
υ	kinematic viscosity

Subscripts

w	condition at wall
∞	condition at infinity

experiment with zero nanoparticle mass flux. It is revealed that while energy and concentration were detrimental, the Hall effects improved the main and secondary velocity profiles. For instance, Jamshed et al. [4] deliberated on unsteady Casson nanofluid flow with solar thermal radiation. The fluid flow was assumed to be occurring through a stretched sheet. In their work, they investigated the influence of slip conditions and solar thermal transitions, as well as entropy, and concluded that regarding heat transmission, the Cu–H_2O nanofluid exceeds the TiO_2–H_2O nanofluid. A convectively heated stretched sheet was supposed to be the flow medium in Kumar et al.'s [5] study of the dual-diffusive flow of Casson MHD nanofluid. It was found that the rate of entropy generation was reduced due to the acceleration of the plastic dynamic viscosity of Casson nanofluid. On the liquefied flow in a magnetic field, the consequences of viscous and Joule dissipations were explained. A study on Darcy Forchheimer bi-convection flow was performed by Siddiqui et al. [6], where Casson nanofluid was considered the base fluid. The behaviour of fluid flows across a revolving, stretched disc in the presence of heat radiation and entropy production is explored. In their research on entropy production in convective fluid flow, Sahoo et al. [7] took radiation in fluid flow into account, along with the emergence of activation energy and Hall current. The finding of this study is entropy generation reduction by incorporating the Brownian motion and thermophoresis parameters. Their investigation's challenge was determined to be multiple regression models with unstable three-dimensional MHD flow. MHD flow of non-Newtonian (Casson) nanofluid through a porous medium has been studied by Abo-Dahab et al. [8], where the porous medium was considered nonlinear and heated. The extending surface effect was deliberate in their work with suction or injection. Ganesh et al. [9] researched radiative Casson MHD nanofluid flow through a nonlinearly extending surface with a Darcy-Forchiemer medium. The chemical reaction was accomplished in that work with thermal radiation. Temperature falls under the influence of Brownian diffusion and radiation, which is the key finding of this work. Ahmed et al. [10] studied the Maxwell fluid flow of hybrid nanofluid through a stretching sheet. The base particles of that hybrid nanofluid were kerosene oil, kerosene oil Go + silver (Ag), or graphene oxide (Go). The flow-related equations were converted into ODEs, and to find the numerical solutions, the Runge-Kutta method was used as a solution procedure with the help of MATLAB coding. Rabbi et al. [11] performed an exploration of the erratic MHD Casson liquefied flow with thermophoresis effects and Brownian motion and discovered that mass transfer declined with increasing the chemical reaction. The effects of nonlinear radiation on heat generation have been studied by Akinshilo et al. [12] On MHD nano-fluid flow with Casson properties, a thin needle has been approached as a flow medium. Nadeem et al. [13] investigated a Reynolds nanofluid of non-Newtonian (Casson) flow past a slanted surface and discovered that the surface thickness parameter acts as a decreasing parameter for velocity and temperature distribution. Mass and heat transmission of Casson nanofluid flow have been researched through a cylindrical wavy channel by Majeed et al. [14]. It has been noted that shifting the walls has reduced the rate of mass, whereas maximisation has occurred in the middle of the cylindrical channel. Shoaib et al. [15] deliberated the behaviour of Casson flow of MHD fluid in the presence of thermal energy under a porous medium past an inclined surface and found that the temperature fell with increasing radiation and concentration diminished with the impact of the chemical process.

The primary process of thermal radiation is the emission of electromagnetic waves from an object's surface as a result of its temperature, typically in the infrared area of the electromagnetic spectrum. The thermal motion of the object's internal constituents, such as atoms and molecules, is what causes this emission of electromagnetic radiation.

Table 1
Comparison of the current article with earlier works.

Authors	Quantities							Solution method
	TR	MHD	CF	SS	NF	TE	TD	FDM
Ali et al. [29]	√	√	×	√	√	√	√	√
Yin et al. [20]	√	√	×	√	√	×	×	×
Farooq et al. [23]	√	×	×	×	√	×	×	×
Swalmeh et al. [26]	√	√	×	×	√	×	×	×
Majeed et al. [14]	×	√	√	×	×	×	×	×
Abd El-Aziz et al. [3]	×	√	√	√	√	√	×	×
Reza-E-Rabbi et al. [11]	√	√	√	√	√	×	√	√
Ganesh et al. [9]	√	√	√	√	√	×	×	×
Khan et al. [35]	√	√	×	×	√	√	√	×
Li et al. [34]	√	√	×	×	√	√	√	×
Recent Article	√	√	√	√	√	√	√	√

Condensed formations: CF (Casson Fluid); MHD (Magnetohydrodynamics); TR (Thermal Radiation); SS (Stretching Sheet); NF (Nano-fluid); TE (Thermoelectric/Hall Current); TD (Time dependant); FDM (Finite Difference Method); √ (Present); × (Absent).

Thermal radiation is the electromagnetic energy that a substance emits as a result of its heat, and the features of this radiation reflect the temperature within the substance. Several implementations, such as optoelectronics, spectroscopy, energy-conversion devices, and thermal management, require an aptitude to control heat emission. Hybrid nanofluid was used as the base fluid in an experiment by Waqas et al. [16] that investigated MHD radiative flow across a spinning disk. The influence of thermal radiation (non-linear) has been described on the hybrid nano-fluid flow, where SWCNT-TiO_2 and MWCNT-$CoFe_2O_4$ particles were mixed as nanometer-sized particles with the fluids, and it was detected that the temperature progressed because of the improvement of the temperature ratio. Patil et al. [17] researched the MHD flow of Prandtl nanofluid with chemical reactions and thermal radiation. The experiment was performed on a heated stretching sheet due to convection. Ghasemi et al. [18] investigated nanofluid flow in the manifestation of magnetic fields as well as nonlinear radiation, where stretching sheets have been considered. It highlights that the Brownian motion acts as an increasing temperature factor. A plane Poiseuille flow of fluid with nanoparticles in the presence of radiation as well as convection has been experimented with by Alamri et al. [19] with porous medium and found that the Stefan blowing factor slowly diminished the velocity and temperature. When Yin et al. [20] studied bi-convection MHD nano-fluid flow under the stimulus of heat radiation through a stretched cylinder, they found that thermophoresis diffusion had lowered the temperature distribution. Also, Mahat et al. [21] analysed the impression of thermal radiation on fluid flow containing viscoelastic Walters'-B along a circular cylinder with constant heat flux and concluded that the velocity and temperature distribution are comparatively higher in constant heat flux than in convective boundary situations. Arithmetical analysis has been executed by Naqvi et al. [22] about hybrid nano-liquid movement with the involvement of entropy generation and thermal radiation. The thermal gradient grows as a result of the Biot number, and it is also noticed that the entropy of the system has improved because of the Reynolds number. Farooq et al. [23] conducted a computational investigation of Williamson nanofluid flow involving Cattaneo–Christov mass and heat flux and observed that the thermal profile drops with Prandtl number but improves with heat source-sink parameter and thermal radiation. Tarakaramu et al. [24] performed a numerical analysis of non-Newtonian MHD nanofluid flow under convective conditions, including nonlinear radiation, and revealed that the results employing the different parameters in the non-Newtonian case are more effective on physical phenomena than the Newtonian case. With the inclusion of thermal radiation, an investigation has been completed by Saeed et al. [25] on hybrid nano-fluid flow in a Darcy–Forchheimer porous medium and established that the hybrid nano-fluid emits heat more lightly than the traditional nano-fluid. Swalmeh et al. [26] also researched Williamson ferrofluid with thermal radiation and magnetic impact and discovered that the velocity and energy transfer improved with increasing the thermal radiation. Another paper [27] has been published on radiative non-Newtonian nanofluid flow, including chemical reactions, and concluded that the thickening fluid deals the maximum velocity for higher material parameters. An unsteady analysis of MHD second-grade fluid flow has been accomplished by Ganjikunta et al. [28] under radiative circumstances and constructed that the increment of the Nusselt number is the impact of the chemical reaction.

The Hall effect, or thermoelectric effect, is the generation of an electric potential (the Hall voltage) throughout an electrical component perpendicular to the conductor's electric current and to a magnetic field that is applied perpendicular to the current. In 1879, Edwin Hall discovered this fact. Ali et al. [29] investigated hydromagnetic nanofluid flow in the presence of thermoelectricity and radiation. It is revealed that the velocity profiles are more enhanced for combined impacts of thermoelectric and radiation than for individual impacts of them. An analysis of nonlinear radiation in a periodic non-Newtonian nanofluid flow has been investigated by Reza-E-Rabbi et al. [30] in terms of the occurrence of Arrhenius activation energy and found that the temperature is controlled by a sinusoidal magnetic field. Authors have also implemented numerical modelling [31] on the flow of a non-Newtonian liquid under the appearance of thermal radiation, which acts non-linearly, and remarked that the nonlinear radiation enhanced the Lorentz force on velocity distribution. Ali et al. [32] also explored the impressions of Hall current and radiation on Bingham fluid and concluded that the impressions of stretching rate are more significant for Bingham fluid than Newtonian fluid. Shamshuddin et al. [33] studied hybrid nanofluid flow with radiation mechanisms and Hall currents and obtained that the velocity profiles are higher for unitary ternary hybrid nanofluid flow than the single (unitary hybrid or ternary hybrid) nanofluid. An exploration of Jeffrey nanofluid flow along a wavy frame under the impacts of Hall effects has been discussed by Li et al. [34], who noticed that the velocity field diminished and boundary layer phenomena improved as the Hall parameter increased. Authors [35] discussed the impacts of Hall current in hybrid nanofluid flow, which is considered radiative, and observed that the radiation parameter enhances the temperature profiles while radial velocity is enhanced by Hall current. Heat transfer analysis in the presence of Hall effects has been developed by Hussain et al. [36] in a rotating system. Another exploration of the thermoelectric (Hall current) and magnetic effects on nanofluid flow with chemical reactions has been accomplished by Khan et al. [37]. It has been noted that higher magnetic fields reduce the velocity distribution while temperature improves with Eckert numbers. In 2021, Khan et al. [38] conducted research on viscous fluid flow and analysed the irreversibility of Darcy-Forchheimer flow. The importance of heat transfer and entropy generation was considered in their experiment, and the behaviour of thermodiffusion was also examined. An unsteady MHD flow was explored by Venkateswarlu et al. [39], which passed past a vertical porous plate. The oscillatory suction velocity was considered in their research work as well as the incompressible viscous fluid, which was electrically conducting. Ali et al. [40] presented the investigation of Dufour and Soret effects on MHD flow, where the fluid was deliberated as an Oldroyd-B nanofluid with rotating flow. Upon the appearance of the dual-diffusing Cattaneo-Christov thermal flux simulation, stretching sheet was also used as the flow medium in their issue. The numerical duality of magnetohydrodynamic motionlessness point flow was analysed by Uddin et al. [41]. The shrinking and stretching sheet has been employed for their experiment to find heat transfer of the nanofluid flow in the depiction of a magnetic field. Kakar et al. [42] presented an investigation on magnetised water-based hybrid nanofluid flow in their work, where stretching sheet was also taken as the flow medium. Two isolated nanoparticles, such as Al_2O_3 and *Cu,* were mixed

with the MHD fluid to make the nanofluid flow. A numerical study on the MHD flow of nanofluid across an exponential stretchable sheet with chemical reaction has been conducted by Gopal et al. [43]. The dynamics of a multistage fluid approaching a stretched sheet containing nanoparticles were explored by Reza-E-Rabbi et al. [44]. The depiction of a chemical reaction on a porous plate has been used by Arifuzzaman et al. [45] to assess the thermal energy transfer and mass transmission of radiative MHD fluid flow. Bhatti et al. [46] worked on thermo-biconvective nano-fluid, which through a Riga plate is the manifestation of Arrhenius activation energy.

As a final point, to compare this latest study with earlier published studies, a tabular representation has also been established in Table 1. Observing the above discussion and seeing the widespread applications of Casson nano-fluids such as food processing, mechanical engineering, chemical engineering, bio-medicine, drag delivery system. The study proposed our research on MHD Casson nano-fluid flow in appearance of thermoelectric and radiation where the fluid flows past a stretching sheet. The primary objective of this paper has been indicated below.

- To establish the mathematical equations for example: continuity, momentum, energy, and concentration, which are related to the problem and the analogous boundary conditions.
- To exchange the dimensional partial differential equations into the dimension less partial differential equations via proper non-dimensional parameters and variables.
- The Finite Difference method will be employed with the help of FORTRAN to get the numerical solutions.
- To search at how incidental characteristics affect temperature, concentration, and velocity, as well as skin friction.
- To analyse the impression of thermoelectric and radiation jointly on velocity and temperature profiles with streamlines and isotherms spectacle for Casson fluids and Newtonian fluids.
- To represent the comparison of the influence of radiation impact and thermoelectric on Newtonian and non-Newtonian fluids.

2. Applications

Consequently, there are several applications for the current study in a variety of industries, including the biomedical, cancer therapy, photoelectric, and security fields. In more detail, it may be argued that the Casson fluid is a member of a non-Newtonian fluid class that displays elastic solid behaviour up to a certain stress threshold before transitioning to liquid behaviour. These fluids are known as viscoelastic fluids and have an extensive uses in engineering, preparing food, drilling, and other industries. Because of its outstanding thermal conductivity, nano-fluid is utilized as a producing fluid (conventional fluids). Several new platforms, such as optoelectronics, energy-conversion devices, thermal management, and spectroscopy, are dependant on their ability to regulate heat radiation. The chemotherapy utilized by the current study is indeed helpful for combating cancer.

3. Methodology

In accordance with a former article, the present article will look into the implications of thermoelectric and radiation on time-dependant non-Newtonian (Casson) and Newtonian nano-fluid flow on a stretchable periphery. An appropriate numerical procedure is necessary to finish this project, which is focused on numerical simulation. For this reason, there has been usage of the explicit finite difference (EFD) method. After the technique is used, the problem is more precisely defined, and a stability test is conducted. The recent project has been categorized in style provided:

- With the use of the fundamental idea of computational fluid dynamics, the boundary layer assumption, and by adhering to the work of Ali et al. [29], a group of governing equations have been generated: continuity, velocity, energy, and concentration.
- The developed equations have been modified as non-dimensional by incorporating a variety of dimensionless elements.
- The specified equations are simply calculated utilizing the EFDM algorithm.
- Comprehensive convergence and stability requirements have been devised to ensure the system is convergent.
- Employing Visual Fortran, a computer program, the numerical data is gathered.
- Tecplot 360 and Microsoft Excel 19 are employed to analyse the numerical data as well as for generating the graphical representation.
- The characteristics of velocity, temperature, concentration, isotherm, streamlines, and other major physical phenomena with the usual look of separate flow fields, are depicted in the findings and discussion section.
- As this investigation is simulation-based, the verification is accomplished by integrating a different simulation-based article that was previously available in the literature.

4. Mathematical analysis

Two-dimensional radiative MHD flow of Casson fluid with nanoparticles and the entrance of thermoelectric in the area $y > 0$ past a stretching plate, where the power-low velocity is considered as $U_0 = ax$, where a represents a non-negative real number. The stretching sheet is placed to be organizing along x-axis and the y-axis is orthogonal to the stretching sheet. A fluid is taken as hot with temperature T_w^* is improved to warm or cold the plane of the stretchable plate in the appearance of thermoelectric and thermal radiation, whose are employed on the MHD nano-fluid flow in the approach of parallel to the x- axis and the initiative magnetic field has been considered. The identical volume fraction (Concentration) of nanoparticle is overwhelmed of the base of the stretching plate is C_w^*, whereas the inclusive concentration as well as temperature are C_∞^* besides T_∞^* respectively.

Casson fluid deals the rheological equations [30] in (1) and (2),

$$\pi_{ij} = \begin{cases} \left(\mu_c + \frac{P_y}{\sqrt{2\pi}}\right) 2\zeta_{ij} \text{as} \pi > \pi_b \\ \left(\mu_c + \frac{P_y}{\sqrt{2\pi_b}}\right) 2\zeta_{ij} \text{as} \pi < \pi_b \text{where}, P_y = \frac{\mu_c \sqrt{2\pi}}{\gamma} \end{cases} \tag{1}$$

$$\therefore \upsilon' = \upsilon\left(1 + \frac{1}{\gamma}\right) \text{with} \upsilon = \frac{\mu_c}{\rho} \tag{2}$$

The aforementioned quantity, μ_c corresponds to the plastic viscosity, ζ_{ij} and π_{ij} are $(i, j)^{\text{th}}$ ingredient the rate of deformation and stress tensor, π_b denoted the critical value of this product, π symbolizes the result of multiplying the deformation rate component by itself and P_y represents the yield stress. Thus, utilising the approximation regarding the boundary layers and taking the aforementioned into account, the set of fundamental equations relating to MHD nano-fluid flow, including momentum, energy, and concentration, is provided [29,47,48] by the Eqs. (3)–(7),

$$\frac{\partial v}{\partial y} + \frac{\partial u}{\partial x} = 0 \tag{3}$$

$$v\frac{\partial u}{\partial y} + \frac{\partial u}{\partial t^*} + u\frac{\partial u}{\partial x} = g\beta^*\left(C^* - C_\infty^*\right) + \upsilon\left(1 + \frac{1}{\gamma}\right)\frac{\partial^2 u}{\partial y^2} - \frac{\sigma B_0^2}{\rho(1+m^2)}(u + mw) + g\beta\left(T^* - T_\infty^*\right) \tag{4}$$

$$v\frac{\partial w}{\partial y} + \frac{\partial w}{\partial t^*} + u\frac{\partial w}{\partial x} = \upsilon\left(1 + \frac{1}{\gamma}\right)\frac{\partial^2 w}{\partial y^2} + \frac{\sigma B_0^2}{\rho(1+m^2)}(mu - w) \tag{5}$$

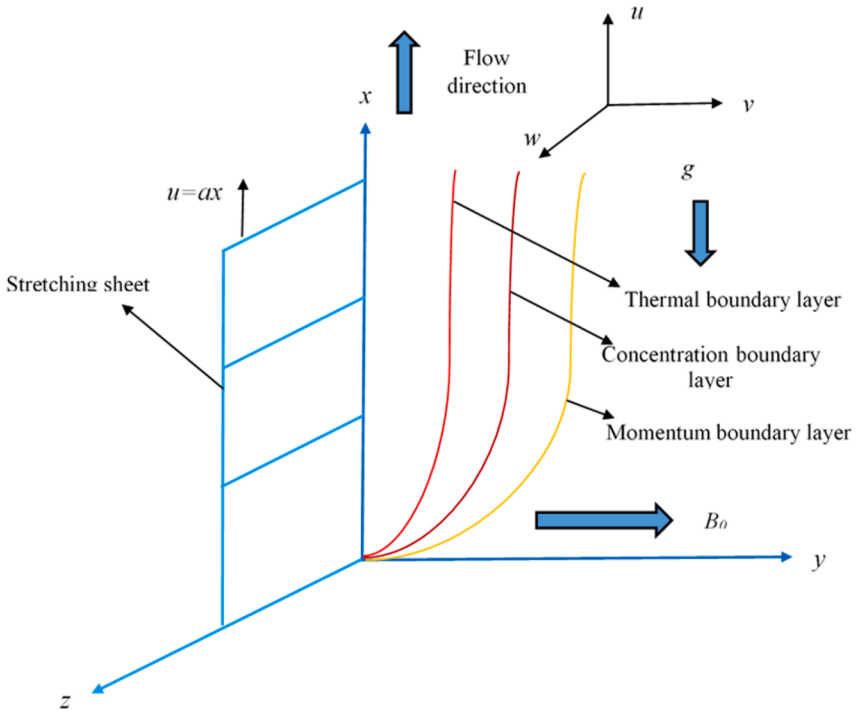

Fig. 1. Physical diagram of the problem [29].

$$v\frac{\partial T^*}{\partial y}+\frac{\partial T^*}{\partial t^*}+u\frac{\partial T^*}{\partial x}=\tau\left\{\frac{D_T}{T^*_\infty}\left(\frac{\partial T^*}{\partial y}\right)^2+D_B\left(\frac{\partial C^*}{\partial y}\frac{\partial T^*}{\partial y}\right)\right\}+\alpha\frac{\partial^2 T^*}{\partial y^2}$$
$$+\frac{\sigma B_0^2}{\rho c_p\left(1+m^2\right)}\left(u^2+w^2\right)+\left(1+\frac{1}{\gamma}\right)\frac{\upsilon}{c_p}\left(\left(\frac{\partial u}{\partial y}\right)^2+\left(\frac{\partial w}{\partial y}\right)^2\right)-\frac{1}{\rho c_p}\frac{\partial q_r}{\partial y} \tag{6}$$

$$v\frac{\partial C^*}{\partial y}+\frac{\partial C^*}{\partial t^*}+u\frac{\partial C^*}{\partial x}=\frac{D_T}{T^*_\infty}\frac{\partial^2 T^*}{\partial y^2}+D_B\frac{\partial^2 C^*}{\partial y^2} \tag{7}$$

Eq. (8) is used to represent the associated boundary conditions for Eqs. (3–7):

$$\left.\begin{array}{l} u=U_0=ax, v=w=0, C=C^*_w, T^*=T^*_w \text{at} y=0 \\ u=v=w=0, C^*\to C^*_\infty, T^*\to T^*_\infty \text{as} y\to\infty \end{array}\right\} \tag{8}$$

where w is the secondary velocity obtained through the use of the Hall current, and u and v symbolized the main velocity phenomena respectively to the x- and y-axes. $t^* \geq 0$ deals the time, ρ represents liquid density, g stands for the acceleration brought on by gravity, B_0 indicates the magnetic induction field, heat capacity under constant pressure is represented by c_p., α is the fluid thermal diffusivity, σ represents the electrical conductivity, D_T and D_B are the thermophoresis propagation coefficient and Brownian propagation coefficient, accordingly., the effective heat capacity of a nanoparticle material is represented by the ratio $\tau(=(\rho c)_p/(\rho c)_f)$, m indicates the Hall current parameter, the kinematic viscosity denoted by υ, The exchange of heat and mass expansion coefficient are presented by β and β^* correspondingly.

In the approximation of Rosseland diffusion for radiative components which has been taken as [29,30]

$$q_r=\frac{-4\sigma^*}{3k^*}\frac{\partial T^{*4}}{\partial y} \tag{9}$$

Where, k^*be the absorption parameter and σ*indicates the Stefan Boltzman constant. The temperature difference is possessed as T^{*4}within the flow, by ignoring the higher order variables, may be enlarged in terms of the Taylor series [29,30].

$$T^{*4}\cong 4T^{*3}_\infty T^*-3T^{*3}_\infty \tag{10}$$

To get the dimension-less form of the problem-related equations and the corresponding boundary conditions, the equation below lists the suggested dimensionless expressions (11) taken as [14,18,29,49],

$$t=\frac{t^*U_0^2}{\upsilon}, X=\frac{xU_0}{\upsilon}, U=\frac{u}{U_0}, Y=\frac{yU_0}{\upsilon}, V=\frac{v}{U_0}, W=\frac{w}{U_0}, T=\frac{T^*-T^*_\infty}{T^*_w-T^*_\infty}, \Pr=\frac{\upsilon}{\alpha}$$
$$C=\frac{C^*-C^*_\infty}{C^*_w-C^*_\infty}, Gr=\frac{g\beta\left(T^*_w-T^*_\infty\right)\upsilon}{U_0^3}, Gm=\frac{g\beta^*\left(C^*_w-C^*_\infty\right)\upsilon}{U_0^3}, M=\frac{\sigma B_0^2\upsilon}{U_0^2\rho}, Le=\frac{\alpha}{D_B} \tag{11}$$
$$N_r=\frac{16\sigma T^{*3}_\infty}{3k^*\kappa}, N_b=\frac{\tau D_B\left(C^*_w-C^*_\infty\right)}{\upsilon}, N_t=\frac{\tau D_T\left(T^*_w-T^*_\infty\right)}{\upsilon T^*_\infty}, Ec=\frac{U_0^2}{c_p\left(T^*_w-T^*_\infty\right)}, J=\frac{\sigma B_0^2\upsilon}{\rho c_p\left(T^*_w-T^*_\infty\right)}$$

where the following parameters and numbers are used in the formula: M, N_r, N_b, N_b, Pr, Ec, Gr, Gm, Le, which stands for magnetic, radiation, Brownian, and thermophoresis parameters as well as Prandtl, Eckert, Grashof, modified Grashof, and Lewis numbers, respectively.

The problem related equations now take the following dimensionless form in Eqs. (12)–(16), where w, v, u, C^*, and T^* are functions of y, x, and

t^*,

$$\frac{\partial V}{\partial Y}+\frac{\partial U}{\partial X}=0 \tag{12}$$

$$\frac{\partial U}{\partial t}=\left(1+\frac{1}{\gamma}\right)\frac{\partial^2 U}{\partial Y^2}-\frac{M}{1+m^2}(U+mW)+GrT+GmC-V\frac{\partial U}{\partial Y}-U\frac{\partial U}{\partial X} \tag{13}$$

$$\frac{\partial W}{\partial t}=\left(1+\frac{1}{\gamma}\right)\frac{\partial^2 W}{\partial Y^2}+\frac{M}{1+m^2}(Um-W)-V\frac{\partial W}{\partial Y}-U\frac{\partial W}{\partial X} \tag{14}$$

$$\frac{\partial T}{\partial t}=\left(\frac{1+N_r}{\Pr}\right)\frac{\partial^2 T}{\partial Y^2}+N_b\frac{\partial C}{\partial Y}\frac{\partial T}{\partial Y}+\left(1+\frac{1}{\gamma}\right)Ec\left(\left(\frac{\partial U}{\partial Y}\right)^2+\left(\frac{\partial W}{\partial Y}\right)^2\right)$$
$$+\frac{J}{1+m^2}\left(U^2+W^2\right)+N_t\left(\frac{\partial T}{\partial Y}\right)^2-V\frac{\partial T}{\partial Y}-U\frac{\partial T}{\partial X} \tag{15}$$

$$\frac{\partial C}{\partial t}=\frac{1}{Le\Pr}\frac{\partial^2 C}{\partial Y^2}+\frac{N_t}{N_b Le\Pr}\frac{\partial^2 T}{\partial Y^2}-V\frac{\partial C}{\partial Y}-U\frac{\partial C}{\partial X} \tag{16}$$

The associated boundary restrictions of the dimensionless equations switch into

$$\left.\begin{array}{l}\text{When} Y=0,\text{then} V=0,T=1,C=1,U=1,W=0\\ \text{When} Y\to\infty,\text{then} C\to 0,T\to 0,U=V=W=0\end{array}\right\} \tag{17}$$

The following are the non-dimensional representations of the three exceptional wonders of fluid flow: local skin friction, rate of mass transfer (i.e., Sherwood number), and rate of heat transfer (i.e., Nusselt number):

$$C_f=\frac{2\tau_w}{\rho U_0^2}=2\left(\frac{\partial U}{\partial Y}\right)_{Y=0} \tag{18}$$

$$Sh=-\frac{x}{C_w^*-C_\infty^*}\left(\frac{\partial C^*}{\partial y}\right)_{y=0}\Rightarrow Sh\mathrm{Re}_x^{-1}=-\left(\frac{\partial C}{\partial Y}\right)_{Y=0} \tag{19}$$

$$Nu=-\frac{x}{T_w^*-T_\infty^*}\left(\frac{\partial T^*}{\partial y}\right)_{y=0}\Rightarrow Nu\mathrm{Re}_x^{-1}=-\left(\frac{\partial T}{\partial Y}\right)_{Y=0} \tag{20}$$

where $\mathrm{Re}_x=(U_0X)\upsilon^{-1}$ represents the Reynolds number.

5. Numerical simulation

In this subsection, the study attempt to simplify the non-dimensional PDE's with the accompanying boundary conditions employing the EFD strategy. It is considered that the height of the stretching sheet $X_{max}=200$ (i.e., X changes from 0 to 200) and consideration $Y_{max}=50$ as resembling to $Y\to\infty$ (i.e., Y changes from 0 to 50). As shown in Fig. 2, it must be utilized that $m=400$ and $n=400$ in the X- and Y-axes grid sectors for the axes and the values of the various parameters have been taken as $Gr=1.00$, $Le=0.55$, $N_b=0.70$, $N_t=0.50$, $M=1.50$, $Gm=2.00$, $N_r=1.50$, $m=0.30$, $Ec=0.30$, $Pr=0.71$ and $\gamma=1.00$.

Now we have the EFD estimation,

$$\begin{array}{l}\left(\frac{\partial U}{\partial Y}\right)_{i,j}=\frac{1}{\Delta Y}\left(U_{i,j+1}-U_{i,j}\right),\left(\frac{\partial U}{\partial t}\right)_{i,j}=\left(U'_{i,j}-U_{i,j}\right)\frac{1}{\Delta t},\left(\frac{\partial U}{\partial X}\right)_{i,j}=\frac{1}{\Delta X}\left(U_{i,j}-U_{i-1,j}\right),\\ \left(\frac{\partial W}{\partial Y}\right)_{i,j}=\frac{W_{i,j+1}-W_{i,j}}{\Delta Y},\left(\frac{\partial W}{\partial X}\right)_{i,j}=\frac{W_{i,j}-W_{i-1,j}}{\Delta X},\left(\frac{\partial W}{\partial t}\right)_{i,j}=\frac{W'_{i,j}-W_{i,j}}{\Delta t},\\ \left(\frac{\partial T}{\partial Y}\right)_{i,j}=\frac{T_{i,j+1}-T_{i,j}}{\Delta Y},\left(\frac{\partial T}{\partial t}\right)_{i,j}=\frac{T'_{i,j}-T_{i,j}}{\Delta t},\left(\frac{\partial T}{\partial X}\right)_{i,j}=\frac{T_{i,j}-T_{i-1,j}}{\Delta X},\\ \left(\frac{\partial C}{\partial Y}\right)_{i,j}=\frac{1}{\Delta Y}\left(C_{i,j+1}-C_{i,j}\right),\left(\frac{\partial C}{\partial X}\right)_{i,j}=\left(C_{i,j}-C_{i-1,j}\right)\frac{1}{\Delta X},\left(\frac{\partial C}{\partial t}\right)_{i,j}=\frac{1}{\Delta t}\left(C'_{i,j}-C_{i,j}\right),\\ \left(\frac{\partial^2 U}{\partial Y^2}\right)_{i,j}=\frac{U_{i,j-1}-2U_{i,j}+U_{i,j+1}}{(\Delta Y)^2},\left(\frac{\partial^2 W}{\partial Y^2}\right)_{i,j}=\frac{W_{i,j-1}-2W_{i,j}+W_{i,j+1}}{(\Delta Y)^2}\\ \left(\frac{\partial^2 T}{\partial Y^2}\right)_{i,j}=\frac{T_{i,j-1}-2T_{i,j}+T_{i,j+1}}{(\Delta Y)^2},\left(\frac{\partial V}{\partial Y}\right)_{i,j}=\frac{1}{\Delta Y}\left(V_{i,j}-V_{i,j-1}\right),\left(\frac{\partial^2 C}{\partial Y^2}\right)_{i,j}=\frac{C_{i,j-1}-2C_{i,j}+C_{i,j+1}}{(\Delta Y)^2},\end{array} \tag{21}$$

Employing the aforementioned equations, evaluate the differential Eqs. (12–16), the following equations has been obtained,

$$\frac{V_{i,j-1}-V_{i,j}}{\Delta Y}=\frac{U_{i,j}-U_{i-1,j}}{\Delta X} \tag{22}$$

$$\begin{array}{l}\frac{U'_{i,j}-U_{i,j}}{\Delta t}=GrT_{i,j}+\left(1+\frac{1}{\gamma}\right)\frac{U_{i,j+1}-2U_{i,j}+U_{i,j-1}}{(\Delta Y)^2}-\frac{M}{1+m^2}\left(U_{i,j}+mW_{i,j}\right)+GmC_{i,j}\\ -V_{i,j}\frac{U_{i,j+1}-U_{i,j}}{\Delta Y}+U_{i,j}\frac{U_{i-1,j}-U_{i,j}}{\Delta X}\\ \therefore U'_{i,j}=U_{i,j}+\Delta t\left[\left(1+\frac{1}{\gamma}\right)\frac{U_{i,j+1}-2U_{i,j}+U_{i,j-1}}{(\Delta Y)^2}+GrT_{i,j}+GmC_{i,j}-\frac{M}{1+m^2}\left(U_{i,j}+mW_{i,j}\right)\right]\\ -\Delta t\left[V_{i,j}\frac{U_{i,j+1}-U_{i,j}}{\Delta Y}+U_{i,j}\frac{U_{i,j}-U_{i-1,j}}{\Delta X}\right]\end{array} \tag{23}$$

$$\frac{W_{i,j}^{'}-W_{i,j}}{\Delta t}=\left(1+\frac{1}{\gamma}\right)\frac{W_{i,j+1}-2W_{i,j}+W_{i,j-1}}{(\Delta Y)^2}+\frac{M}{1+m^2}\left(mU_{i,j}-W_{i,j}\right)$$
$$-V_{i,j}\frac{W_{i,j+1}-W_{i,j}}{\Delta Y}-U_{i,j}\frac{W_{i,j}-W_{i-1,j}}{\Delta X}$$
$$\therefore W_{i,j}^{'}=W_{i,j}+\Delta t\left[\frac{M}{1+m^2}\left(mU_{i,j}-W_{i,j}\right)+\left(1+\frac{1}{\gamma}\right)\frac{W_{i,j-1}-2W_{i,j}+W_{i,j+1}}{(\Delta Y)^2}\right]$$
$$-\Delta t\left[V_{i,j}\frac{W_{i,j+1}-W_{i,j}}{\Delta Y}+U_{i,j}\frac{W_{i,j}-W_{i-1,j}}{\Delta X}\right] \tag{24}$$

$$\frac{T_{i,j}^{'}-T_{i,j}}{\Delta t}=N_b\frac{T_{i,j+1}-T_{i,j}}{\Delta Y}\frac{C_{i,j+1}-C_{i,j}}{\Delta Y}+\left(\frac{1+N_r}{\mathrm{Pr}}\right)\frac{T_{i,j+1}-2T_{i,j}+T_{i,j-1}}{(\Delta Y)^2}+N_t\left(\frac{T_{i,j+1}-T_{i,j}}{\Delta Y}\right)^2$$
$$+\frac{J}{1+m^2}\left(U_{i,j}^2+W_{i,j}^2\right)+\left(1+\frac{1}{\gamma}\right)Ec\left(\left(\frac{U_{i,j+1}-U_{i,j}}{\Delta Y}\right)^2+\left(\frac{W_{i,j+1}-W_{i,j}}{\Delta Y}\right)^2\right)$$
$$-U_{i,j}\frac{T_{i,j}-T_{i-1,j}}{\Delta X}-V_{i,j}\frac{T_{i,j+1}-T_{i,j}}{\Delta Y}$$
$$\therefore T_{i,j}^{'}=T_{i,j}+\Delta t\left[N_b\frac{T_{i,j}-T_{i,j+1}}{\Delta Y}\frac{C_{i,j}-C_{i,j+1}}{\Delta Y}+\left(\frac{1+N_r}{\mathrm{Pr}}\right)\frac{T_{i,j+1}-2T_{i,j}+T_{i,j-1}}{(\Delta Y)^2}+N_t\left(\frac{T_{i,j+1}-T_{i,j}}{\Delta Y}\right)^2\right]$$
$$-\Delta t\left[\left(T_{i,j+1}-T_{i,j}\right)\frac{V_{i,j}}{\Delta Y}-\left(1+\frac{1}{\gamma}\right)Ec\left(\left(\frac{U_{i,j+1}-U_{i,j}}{\Delta Y}\right)^2+\left(\frac{W_{i,j+1}-W_{i,j}}{\Delta Y}\right)^2\right)+U_{i,j}\frac{T_{i,j}-T_{i-1,j}}{\Delta X}\right]$$
$$+\frac{J}{1+m^2}\left(U_{i,j}^2+W_{i,j}^2\right)\Delta t \tag{25}$$

$$\frac{C_{i,j}^{'}-C_{i,j}}{\Delta t}=\frac{N_t}{\mathrm{Pr}N_bLe}\frac{T_{i,j+1}-2T_{i,j}+T_{i,j-1}}{(\Delta Y)^2}+\frac{1}{\mathrm{Pr}Le}\frac{C_{i,j-1}-2C_{i,j}+C_{i,j+1}}{(\Delta Y)^2}$$
$$-U_{i,j}\frac{C_{i,j}-C_{i-1,j}}{\Delta X}-V_{i,j}\frac{C_{i,j+1}-C_{i,j}}{\Delta Y}$$
$$\therefore C_{i,j}^{'}=C_{i,j}+\Delta t\left[\frac{1}{\mathrm{Pr}Le}\frac{C_{i,j+1}-2C_{i,j}+C_{i,j-1}}{(\Delta Y)^2}+\frac{N_t}{\mathrm{Pr}N_bLe}\frac{T_{i,j-1}-2T_{i,j}+T_{i,j+1}}{(\Delta Y)^2}\right]$$
$$-\Delta t\left[V_{i,j}\frac{C_{i,j+1}-C_{i,j}}{\Delta Y}+U_{i,j}\frac{C_{i,j}-C_{i-1,j}}{\Delta X}\right] \tag{26}$$

6. Stability and convergence test

Examination of the convergence and stability tests must be conducted out in order to obtain precise numerical solutions using the finite difference methodology. It is feasible to complete the stability test for actual mesh sizes in the following way. As Eq. (22) does not depend onΔt, it may be ignored. It is considered that $e^{i\alpha X}e^{i\beta Y}$ are the ordinary form of expanding Fourier space for *U, W, T* and *C* at an arbitrary time *t* = 0, where$i=\sqrt{-1}$. The elements above change at time *t*,

$$U=E(t)e^{i\alpha X}e^{i\beta Y};W=F(t)e^{i\alpha X}e^{i\beta Y};T=G(t)e^{i\alpha X}e^{i\beta Y};C=H(t)e^{i\alpha X}e^{i\beta Y} \tag{27}$$

The phrases above are altered as follows after the time interval:

$$U=E^{'}(t)e^{i\alpha X}e^{i\beta Y};W=F^{'}(t)e^{i\alpha X}e^{i\beta Y};T=G^{'}(t)e^{i\alpha X}e^{i\beta Y};C=H^{'}(t)e^{i\alpha X}e^{i\beta Y} \tag{28}$$

Now by substituting the Eqs. (27) and (28) in Eqs. (23)–(26), we get

$$\frac{(E^{'}-E)e^{i\alpha X}e^{i\beta Y}}{\Delta t}=\left(1+\frac{1}{\gamma}\right)\frac{2Ee^{i\alpha X}e^{i\beta Y}(\cos\beta\Delta Y-1)}{(\Delta Y)^2}+GrGe^{i\alpha X}e^{i\beta Y}+GmHe^{i\alpha X}e^{i\beta Y}$$
$$-\frac{M}{1+m^2}(E+mF)e^{i\alpha X}e^{i\beta Y}-V\frac{E(e^{i\beta\Delta Y}-1)e^{i\alpha X}e^{i\beta Y}}{\Delta Y}-U\frac{E(1-e^{-i\alpha\Delta X})e^{i\alpha X}e^{i\beta Y}}{\Delta X}$$
$$E^{'}=E\left[1+\frac{2(\cos\beta\Delta Y-1)}{(\Delta Y)^2}\left(1+\frac{1}{\gamma}\right)\Delta t-V\frac{(e^{i\beta\Delta Y}-1)}{\Delta Y}\Delta t-U\frac{(1-e^{-i\alpha\Delta X})}{\Delta X}\Delta t\right]$$
$$+GrG\Delta t+GmH\Delta t-\frac{M}{1+m^2}(E+mF)\Delta t$$
$$\therefore E^{'}=A_1E+A_2F+A_3G+A_4H \tag{29}$$

Here,

$$A_1=1+\left[\frac{2(\cos\beta\Delta Y-1)}{(\Delta Y)^2}\left(1+\frac{1}{\gamma}\right)-V\frac{(e^{i\beta\Delta Y}-1)}{\Delta Y}-U\frac{(1-e^{-i\alpha\Delta X})}{\Delta X}-\frac{M}{1+m^2}\right]\Delta t$$
$$A_2=-\frac{Mm}{1+m^2}\Delta t;A_3=Gr\Delta t;A_4=Gm\Delta t \tag{30}$$

$$\frac{(F^{'}-F)e^{i\alpha X}e^{i\beta Y}}{\Delta t}=\left(1+\frac{1}{\gamma}\right)\frac{2Fe^{i\alpha X}e^{i\beta Y}(\cos\beta\Delta Y-1)}{(\Delta Y)^2}+\frac{M}{1+m^2}(mE-F)e^{i\alpha X}e^{i\beta Y}$$
$$-V\frac{(e^{i\beta\Delta Y}-1)Fe^{i\alpha X}e^{i\beta Y}}{\Delta Y}-U\frac{F(1-e^{-i\alpha\Delta X})e^{i\alpha X}e^{i\beta Y}}{\Delta X}$$
$$F^{'}=F\left[1+\left\{\frac{2(\cos\beta\Delta Y-1)}{(\Delta Y)^2}\left(1+\frac{1}{\gamma}\right)-V\frac{(e^{i\beta\Delta Y}-1)}{\Delta Y}-U\frac{(1-e^{-i\alpha\Delta X})}{\Delta X}\right\}\Delta t\right]$$
$$+\frac{M}{1+m^2}(mE-F)\Delta t$$
$$\therefore F^{'}=A_5E+A_6F \tag{31}$$

Here,

$$A_5=\frac{Mm}{1+m^2}\Delta t$$
$$A_6=1+\left\{\frac{2(\cos\beta\Delta Y-1)}{(\Delta Y)^2}\left(1+\frac{1}{\gamma}\right)-V\frac{(e^{i\beta\Delta Y}-1)}{\Delta Y}-U\frac{(1-e^{-i\alpha\Delta X})}{\Delta X}-\frac{M}{1+m^2}\right\}\Delta t \tag{32}$$

$$\frac{(G^{'}-G)e^{i\alpha X}e^{i\beta Y}}{\Delta t}=\left(\frac{1+N_r}{\mathrm{Pr}}\right)\frac{2Ge^{i\alpha X}e^{i\beta Y}(\cos\beta\Delta Y-1)}{(\Delta Y)^2}+N_b\frac{G(e^{i\beta\Delta Y}-1)e^{i\alpha X}e^{i\beta Y}}{\Delta Y}$$
$$\frac{(e^{i\beta\Delta Y}-1)He^{i\alpha X}e^{i\beta Y}}{\Delta Y}+N_t\left(\frac{G(e^{i\beta\Delta Y}-1)e^{i\alpha X}e^{i\beta Y}}{\Delta Y}\right)^2-U\frac{G(1-e^{-i\alpha\Delta X})e^{i\alpha X}e^{i\beta Y}}{\Delta X}$$
$$+\left\{\left(\frac{E(e^{i\beta\Delta Y}-1)e^{i\alpha X}e^{i\beta Y}}{\Delta Y}\right)^2+\left(\frac{F(e^{i\beta\Delta Y}-1)e^{i\alpha X}e^{i\beta Y}}{\Delta Y}\right)^2\right\}\left(1+\frac{1}{\gamma}\right)Ec-V\frac{G(e^{i\beta\Delta Y}-1)e^{i\alpha X}e^{i\beta Y}}{\Delta Y}$$
$$\frac{J}{1+m^2}\left\{\left(Ee^{i\alpha X}e^{i\beta Y}\right)^2+\left(Fe^{i\alpha X}e^{i\beta Y}\right)^2\right\} \tag{33}$$
$$G^{'}=G[1+\{\frac{2(\cos\beta\Delta Y-1)}{(\Delta Y)^2}\left(\frac{1+N_r}{\mathrm{Pr}}\right)+N_bC\frac{\left(e^{i\beta\Delta Y}-1\right)^2}{(\Delta Y)^2}+N_tT\left(\frac{(e^{i\beta\Delta Y}-1)}{\Delta Y}\right)^2-V\frac{(e^{i\beta\Delta Y}-1)}{\Delta Y}$$
$$-U\frac{(1-e^{-i\alpha\Delta X})}{\Delta X}\}\Delta t]+\left(\frac{(e^{i\beta\Delta Y}-1)}{\Delta Y}\right)^2\left(1+\frac{1}{\gamma}\right)Ec(UE+WF)\Delta t+\frac{J}{1+m^2}(UE+WF)\Delta t$$
$$\therefore G^{'}=A_7E+A_8F+A_9G$$

Here,

$$A_7=\left(1+\frac{1}{\gamma}\right)EcU\left(\frac{(e^{i\beta\Delta Y}-1)}{\Delta Y}\right)^2\Delta t+\frac{J}{1+m^2}U\Delta t,$$
$$A_8=\left(1+\frac{1}{\gamma}\right)EcW\left(\frac{(e^{i\beta\Delta Y}-1)}{\Delta Y}\right)^2\Delta t+\frac{J}{1+m^2}W\Delta t$$
$$A_9=1+N_bC\frac{\left(e^{i\beta\Delta Y}-1\right)^2}{(\Delta Y)^2}\Delta t+\left(\frac{1+N_r}{\mathrm{Pr}}\right)\frac{2(\cos\beta\Delta Y-1)}{(\Delta Y)^2}\Delta t \tag{34}$$
$$+N_tT\left(\frac{(e^{i\beta\Delta Y}-1)}{\Delta Y}\right)^2\Delta t-V\frac{(e^{i\beta\Delta Y}-1)}{\Delta Y}\Delta t-U\frac{(1-e^{-i\alpha\Delta X})}{\Delta X}\Delta t$$

$$\frac{(H^{'}-H)e^{i\alpha X}e^{i\beta Y}}{\Delta t}=\frac{1}{\mathrm{Pr}Le}\frac{2He^{i\alpha X}e^{i\beta Y}(\cos\beta\Delta Y-1)}{(\Delta Y)^2}+\frac{N_t}{\mathrm{Pr}N_bLe}\frac{2Ge^{i\alpha X}e^{i\beta Y}(\cos\beta\Delta Y-1)}{(\Delta Y)^2}$$
$$-V\frac{H(e^{i\beta\Delta Y}-1)e^{i\alpha X}e^{i\beta Y}}{\Delta Y}-U\frac{H(1-e^{-i\alpha\Delta X})e^{i\alpha X}e^{i\beta Y}}{\Delta X}$$
$$H^{'}=H\left[1-V\frac{(e^{i\beta\Delta Y}-1)}{\Delta Y}\Delta t+\frac{1}{\mathrm{Pr}Le}\frac{2(\cos\beta\Delta Y-1)}{(\Delta Y)^2}\Delta t-U\frac{(1-e^{-i\alpha\Delta X})}{\Delta X}\Delta t\right] \tag{35}$$
$$+\frac{N_t}{\mathrm{Pr}N_bLe}\frac{2G(\cos\beta\Delta Y-1)}{(\Delta Y)^2}\Delta t$$
$$\therefore H^{'}=A_{10}G+A_{11}H$$

Here,

$$A_{10}=\frac{2N_t}{\mathrm{Pr}N_bLe}(\cos\beta\Delta Y-1)(\Delta Y)^{-2}\Delta t$$
$$A_{11}=1+\frac{1}{\mathrm{Pr}Le}\frac{2(\cos\beta\Delta Y-1)}{(\Delta Y)^2}\Delta t-V\frac{(e^{i\beta\Delta Y}-1)}{\Delta Y}\Delta t-U\frac{(1-e^{-i\alpha\Delta X})}{\Delta X}\Delta t \tag{36}$$

The Eqs. (29), (31), (33) and (35) can resemble the form of a matrix by Eq. (37),

$$\begin{bmatrix}E^{'}\\F^{'}\\G^{'}\\H^{'}\end{bmatrix}=\begin{bmatrix}A_1&A_2&A_3&A_4\\A_5&A_6&0&0\\A_7&A_8&A_9&0\\0&0&A_{10}&A_{11}\end{bmatrix}\begin{bmatrix}E\\F\\G\\H\end{bmatrix}\therefore\eta^{'}=A_M\eta \tag{37}$$

where

$$\eta^{'}=\begin{bmatrix}E^{'}\\F^{'}\\G^{'}\\H^{'}\end{bmatrix},A_M=\begin{bmatrix}A_1&A_2&A_3&A_4\\A_5&A_6&0&0\\A_7&A_8&A_9&0\\0&0&A_{10}&A_{11}\end{bmatrix}\text{and}\eta=\begin{bmatrix}E\\F\\G\\H\end{bmatrix} \tag{38}$$

The study becomes quite challenging because of the diversity ofA_M. A quick time action i.e., $\Delta t\to 0$ was taken as a consequence, and for this regard, we obtainA_2,A_3,A_4,A_5,A_7,$A_8$and A_{10} all tends to zero. Hence,

$$A_M=\begin{bmatrix}A_1&0&0&0\\0&A_6&0&0\\0&0&A_9&0\\0&0&0&A_{11}\end{bmatrix} \tag{39}$$

The eigenvalues for the above matrix in Eq. (39) are $\lambda_1=A_1$,$\lambda_2=A_6$,$\lambda_3=A_9$ and$\lambda_4=A_{11}$, these data values must gratify the stability conditions which are given by the Eq. (40),

$$|A_1|\le 1,|A_6|\le 1,|A_9|\le 1\text{and}|A_{11}|\le 1 \tag{40}$$

Again, let us consider the given relations,

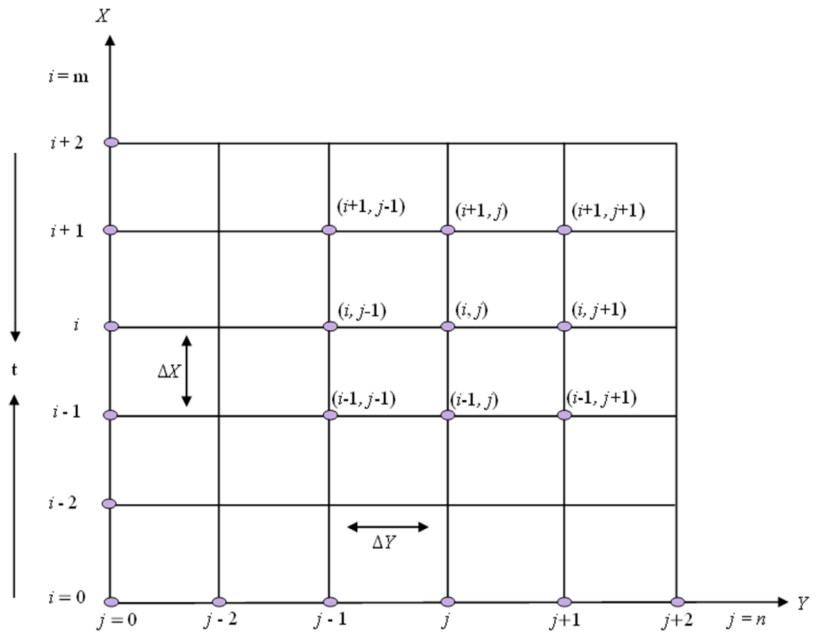

Fig. 2. Finite difference grid in space [30].

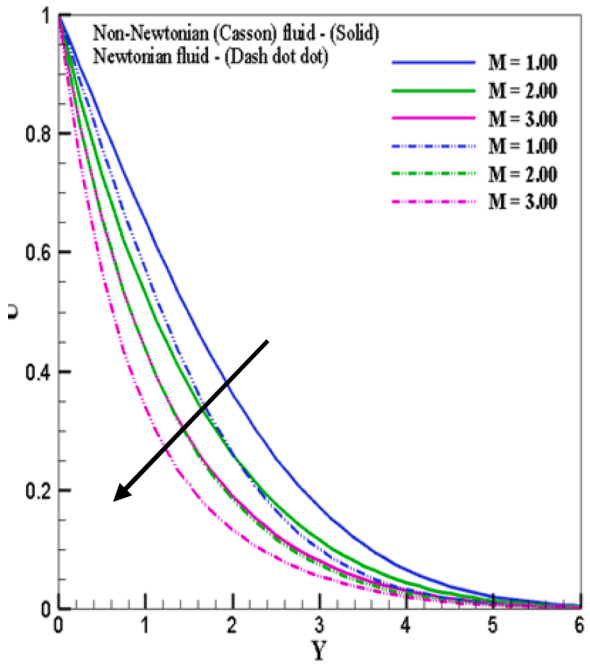

Fig. 3. Impacts of M on primary velocity U.

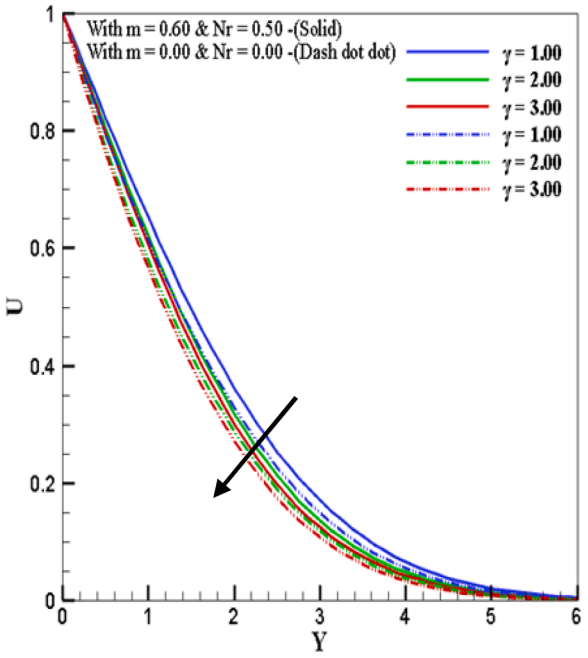

Fig. 4. Influence of γ on primary velocity U.

$$a = \Delta t, b = U\frac{\Delta t}{\Delta X}, c = |-V|\frac{\Delta t}{\Delta Y}, d = 2\frac{\Delta t}{(\Delta Y)^2} \tag{41}$$

In this case, the values of U as well as V are alternately negative as well as positive, where real and non-negative elements are defined as a, b, c, and d. Consequently, the supreme modulus of A_1, A_6, A_9 and A_{11} can be obtained for $\alpha\Delta X = m\pi$ and $\beta\Delta Y = n\pi$with m and n are odd integer. Now substituting the Eqs. (41) in Eqs. (30), (32), (34) and (36), we get

$$A_1 = 1 - 2\left[\frac{M}{1+m^2}a + b + c + \left(1+\frac{1}{\gamma}\right)d\right] \tag{42}$$

$$A_6 = 1 - 2\left[\frac{M}{1+m^2}a + b + c + \left(1+\frac{1}{\gamma}\right)d\right] \tag{43}$$

$$A_9 = 1 - 2\left[\left(\frac{1+N_r}{\mathrm{Pr}}\right)d - N_b C d - N_t T d + c + b\right] \tag{44}$$

$$A_{11} = 1 - 2\left[\frac{1}{\mathrm{Pr}Le}d + c + b\right] \tag{45}$$

To gratifies the feasible values are $A_1 = -1$, $A_6 = -1$, $A_9 = -1$ and $A_{11} = -1$. Hence, the Eqs. (46), (47), (48), and (49) can all be utilized to represent the stability ambience of the problem,

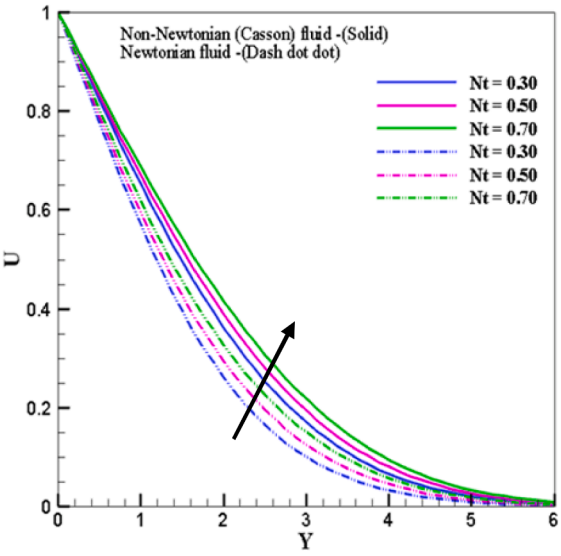

Fig. 5. Effect of *Nt* on primary velocity *U*.

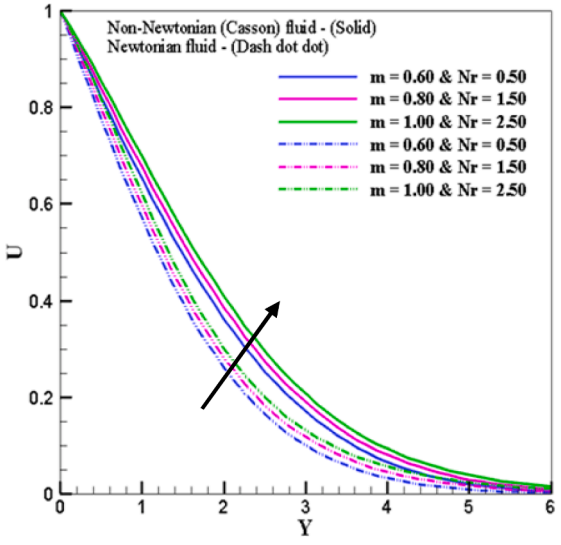

Fig. 6. Combined impacts of m and N_r on primary velocity U.

$$2\left(1+\frac{1}{\gamma}\right)\frac{\Delta t}{(\Delta Y)^2}+V\frac{\Delta t}{\Delta Y}+\frac{M}{1+m^2}\Delta t+U\frac{\Delta t}{\Delta X}\leq 1 \tag{46}$$

$$2\left(1+\frac{1}{\gamma}\right)\frac{\Delta t}{(\Delta Y)^2}+\frac{M}{1+m^2}\Delta t+U\frac{\Delta t}{\Delta X}+V\frac{\Delta t}{\Delta Y}\leq 1 \tag{47}$$

$$2\left[\left(\frac{1+N_r}{\mathrm{Pr}}\right)-N_bC-N_tT\right]\frac{\Delta t}{(\Delta Y)^2}+V\frac{\Delta t}{\Delta Y}+U\frac{\Delta t}{\Delta X}\leq 1 \tag{48}$$

$$\frac{2}{\mathrm{Pr}Le}\frac{\Delta t}{(\Delta Y)^2}+V\frac{\Delta t}{\Delta Y}+U\frac{\Delta t}{\Delta X}\leq 1 \tag{49}$$

At fundamental boundary conditions and at the values of$\Delta X = 0.50$, $\Delta t = 0.001$, and$\Delta Y = 0.125$ the convergence covenant for the existing work would be founded for $\mathrm{Pr} \geq 0.32$ and$Le \geq 0.40$.

7. Results and discussions

With the assistance of graphics and explanations, the numerical simulation of the aforementioned problem is presented in this subsection in a desirable manner. The behaviour of MHD flow of Casson nano-fluid past a stretching plate is beautifully presented in which the primary velocity, secondary velocity, heat, and concentration have been discussed in the emergence of thermoelectric and thermal radiation. The EFD method has been used for this numerical solution and Tecplot-360 software has been used to illustrate this solution with the help of diagram. To explain in detail of the numerical outcomes the various physical quantities of this model such as the velocity, temperature and concentrations profiles are discussed as well as the Streamlines and isotherm with respect to various parameters.

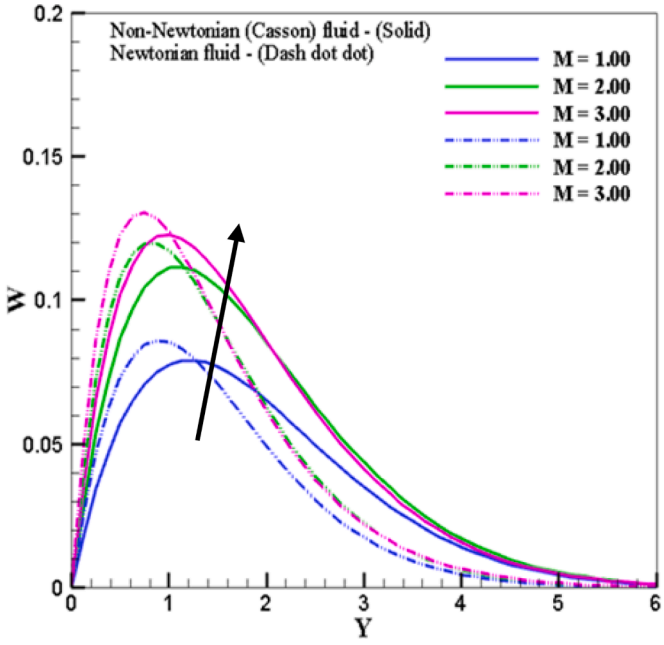

Fig. 7. Variations of secondary velocity profiles *W* caused by *M*.

Fig. 3 illustrates that the primary velocity profiles decrease like in the articles [29,50,51] for both cases, i.e., Newtonian fluid and non-Newtonian (Casson) fluid, since the magnetic parameter M has increased. At $Y = 1.50376$, the values of the primary velocity of non-Newtonian (Casson) fluid are 0.49464, 0.37323, and 0.28672 for the corresponding magnetic parameters $M = 1$, 2, and 3, whereas for Newtonian fluid the corresponding velocities are 0.39407, 0.28331, and

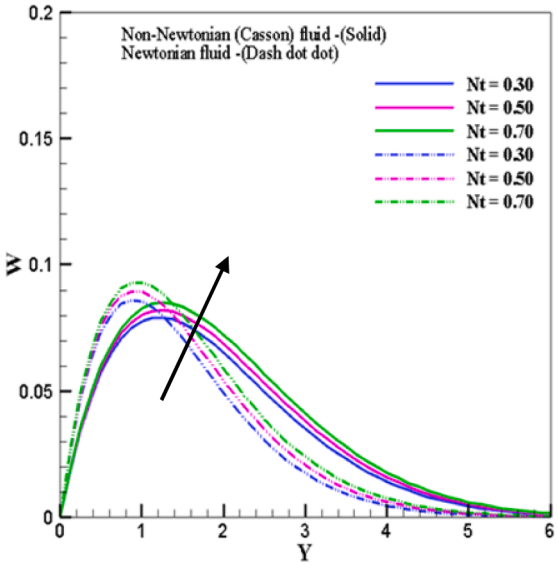

Fig. 8. Variations of secondary velocity profiles *W* caused by N_t.

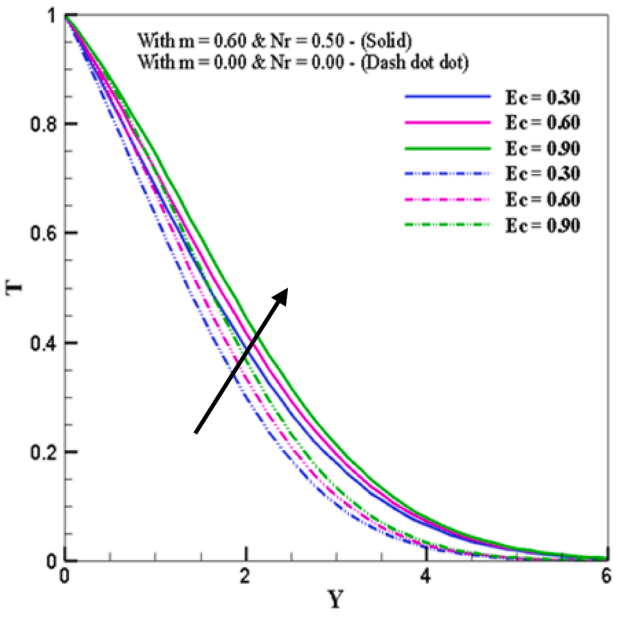

Fig. 9. Deviation of temperature profiles T because of Ec.

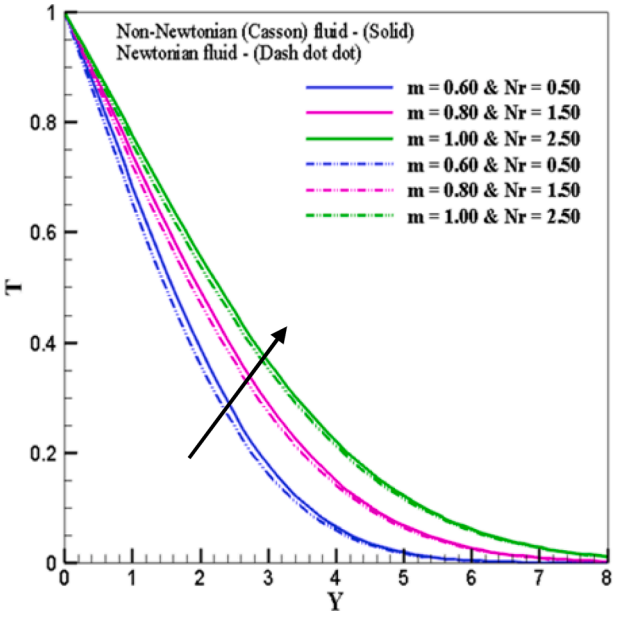

Fig. 10. Deviation of temperature profiles T because of m and N_r, jointly.

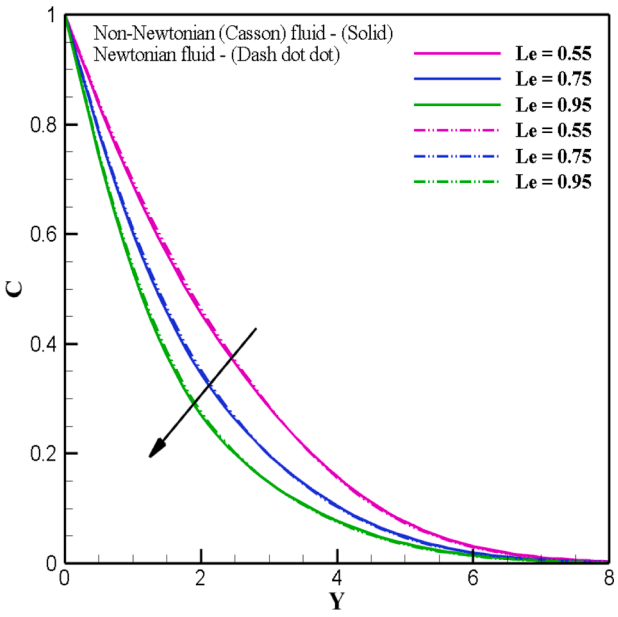

Fig. 11. Behaviour of concentration profiles C caused by Le.

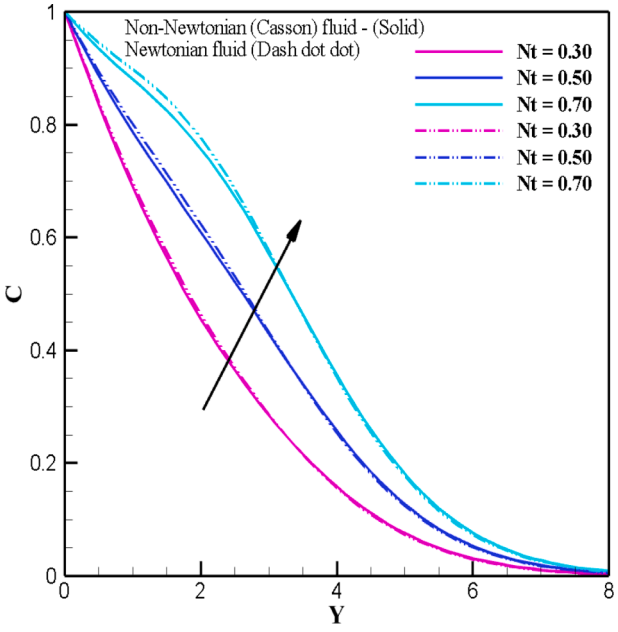

Fig. 12. Nature of concentration profiles C due to change of N_t.

0.20764. The decreasing rate of non-Newtonian (Casson) fluid is 12.14 %, while the rate of Newtonian fluid is 11.07 % from the value $M = 1.00$ to 2.00. Notably, the velocities of non-Newtonian (Casson) fluid are comparatively high compared to Newtonian fluid, and the decline rate is also high. The main reason for decreasing velocity is the Lorentz force, which serves as a barrier. and it is generated by the magnetic field. This breakthrough has found practical applications in hard drives, MRI machines, electric motors, generators, compasses, and various data storage devices.

In Fig. 4, it has been noted that the primary velocity profiles drop significantly for both cases, i.e., the interaction of radiation and Hall current (solid lines) and the absence of Hall current and radiation (dash dot lines), with the increasing of the Casson parameter. This data demonstrates a strong correlation with the previously published article [30,52]. At $Y = 1.50376$, the values of the primary velocity with the presence of Hall current and radiation are 0.49464, 0.45294, and 0.43584 with increasing the Casson parameter from 1 to 3, whereas in the absence of Hall current and radiation, the corresponding velocities are 0.45707, 0.41627, and 0.39976. It is observed that the velocities are comparatively high when thermoelectric and radiation are present. Increasing the Casson parameter in a non-Newtonian fluid raises its yield stress and alters its behaviour. This can reduce fluid velocity, especially at low shear rates, making it harder to move until a higher threshold is reached. Understanding the Casson parameter is crucial for systems using non-Newtonian fluids in industries like food processing, pharmaceuticals, and oil and gas drilling.

Fig. 5 illustrates how the thermophoresis parameter N_t affects the primary velocity profile. It is noticeable that for both fluids, the primary velocity rises when N_t is elevated. But the magnitudes of the velocities for non-Newtonian (Casson) fluid are more significant than those for Newtonian fluid. The concomitant repercussions of radiation N_r and

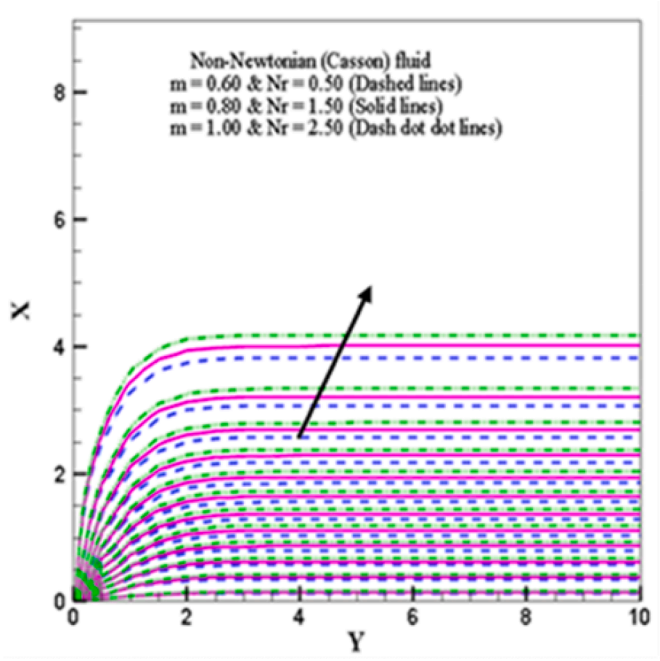

Fig. 13. Stream lines for Non-Newtonian (Casson) fluid with changing N_r and m, jointly.

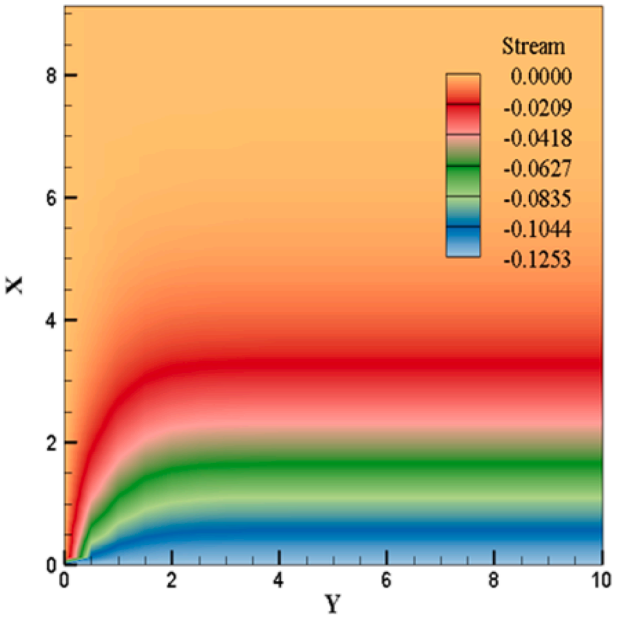

Fig. 14. Flood characterization of Fig. 13.

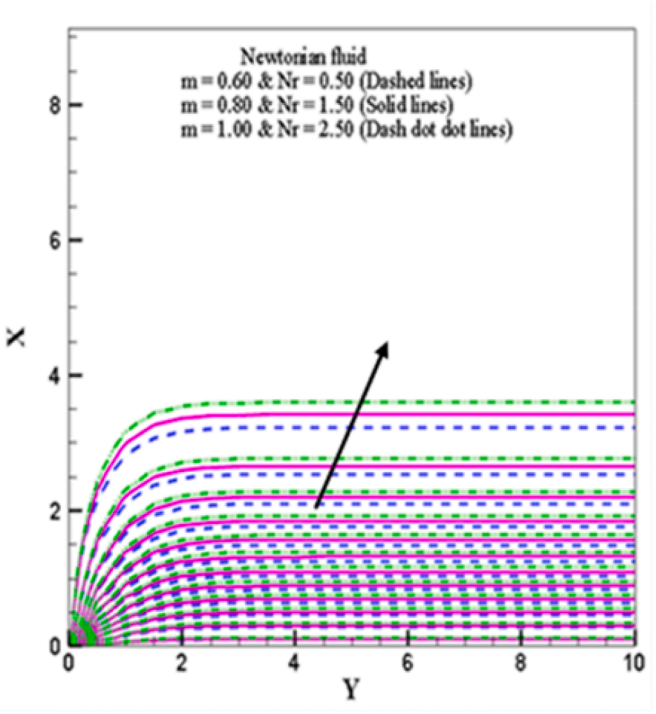

Fig. 15. Stream lines for Newtonian fluid with changing N_r and m, jointly.

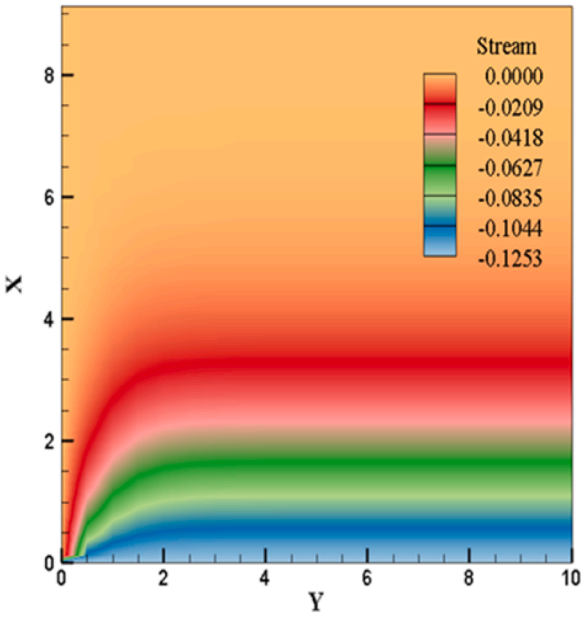

Fig. 16. Flood illustration of Fig. 15.

thermoelectric m on the velocity profile are displayed in Fig. 6, as is the fact that the primary velocity improves with the improvement of radiation parameter N_r and thermoelectric (Hall current) m combined for both fluids. It is also observed that the values of velocities for non-Newtonian (Casson) fluid are comparatively higher than those for Newtonian fluid. This result shows a significant association between Hall's current and the earlier articles [29,50,51]. Fluid interactions become complicated as a result of the combined rise in radiation and Hall current. While stronger Hall currents cause motion, more radiation boosts temperatures and alters density. This has uses in improving technology, cosmological study, propulsion and energy studies, and space science.

In Fig. 7, it is realised that the secondary velocity outlines growth for both cases, i.e., Newtonian fluid and non-Newtonian (Casson) fluid, due to the growth of the magnetic factor M. At peak points, the values of the secondary velocity of non-Newtonian (Casson) fluid are 0.07914, 0.11166, and 0.12285 for the corresponding magnetic parameters M = 1, 2, and 3, whereas for Newtonian fluid the corresponding velocities are 0.08597, 0.11981, and 0.13070. The increasing rate of non-Newtonian (Casson) fluid is 2.18 %, while the rate of Newtonian fluid is 2.24 % from the value M = 1.00 to 3.00. It is clearly notable that the velocities of non-Newtonian (Casson) fluid are comparatively low compared to Newtonian fluid, and the improvement rate is also low. Fig. 8 shows the impacts of thermophoresis on secondary velocity profiles. The secondary velocity profiles are shown to grow with an increase in the

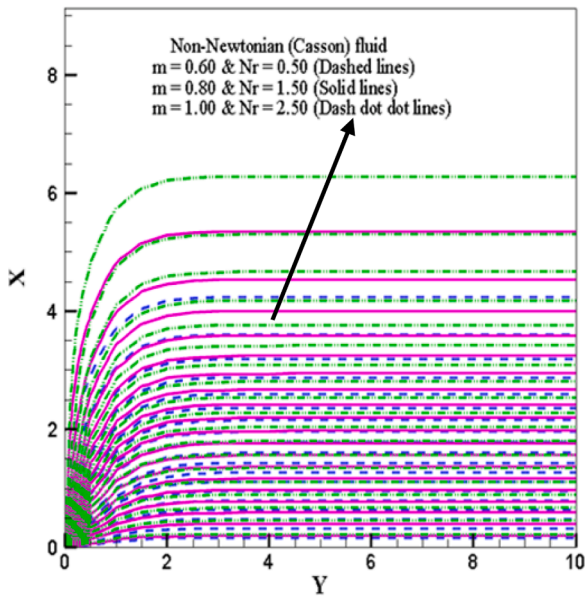

Fig. 17. Isothermal lines for Non-Newtonian (Casson) fluid with changing N_r and m, jointly.

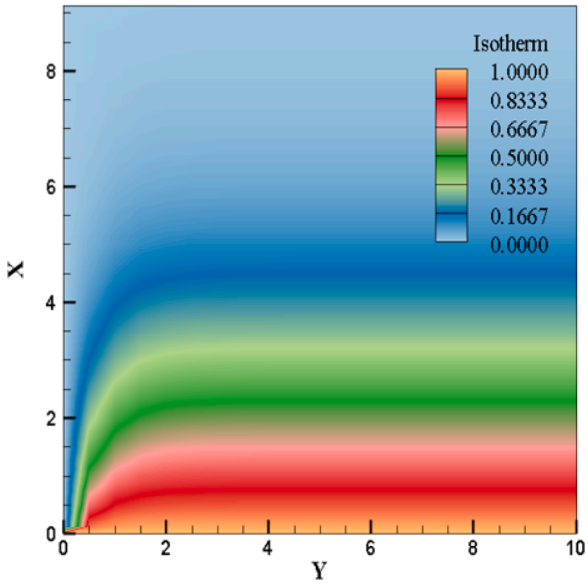

Fig. 18. Flood portrayal of Fig. 17.

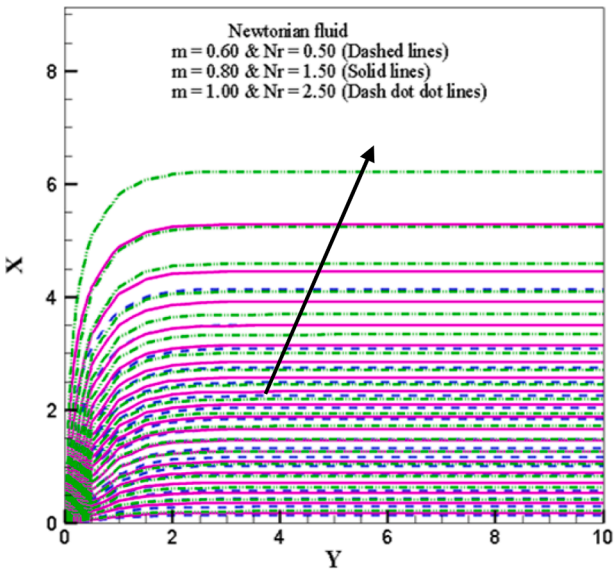

Fig. 19. Isothermal lines for Newtonian fluid with changing N_r and m, jointly.

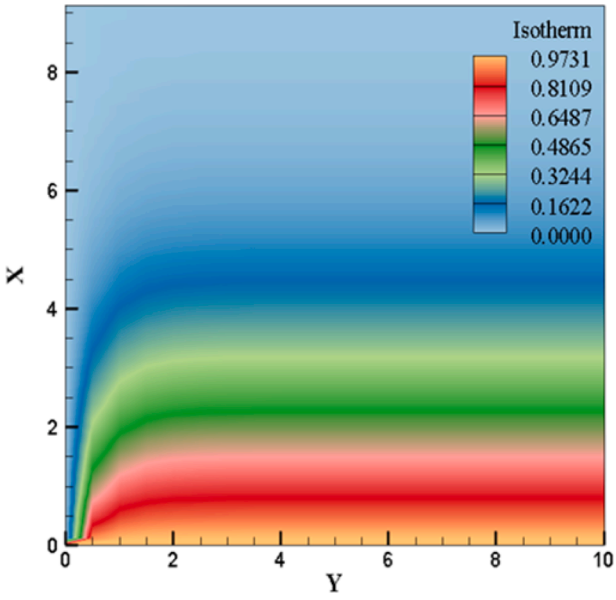

Fig. 20. Flood depiction of Fig. 19.

thermophoresis parameter *Nt* for both fluids. But it is clearly observed that near the boundary layer, i.e., at $Y < 1.50376$, the velocity magnitudes for Newtonian fluid are higher when compared to non-Newtonian fluid, whereas at $Y > 1.50376$, the magnitudes of the velocity for Newtonian fluid are lower than those for non-Newtonian fluid. The thermophoretic force acting on suspended particles is strengthened when the therophoresis parameter is increased, resulting in an amplified secondary velocity in response to temperature gradients. This effect is important for fluid dynamics, heat transmission, and particle management, and it has applications in thermal engineering, microfluidics, and other fields.

The stimulus of Eckert number *Ec* on temperature profiles *T* has been described in Fig. 9. It is apparent that the temperature profiles *T* develop in both cases—that is, when radiation *Nr* and Hall current *m* are active (solid lines) and when they aren't (dash dot lines). A higher Eckert number denotes more heat dissipation occurring inside the fluid flow. As a result, more kinetic energy is converted into heat, raising the temperature of the fluid. In the face of radiation and Hall current, it has been noted that the temperature profiles are higher than the temperature profiles without including the radiation and Hall current. At $Y = 2.50627$, the magnitudes of the temperature are 0.26942, 0.29266, and 0.31583 with $m = 0.60$ and $Nr = 0.50$ for the Eckert number $Ec = 0.30$, 0.60, and 0.90, whereas with the value of thermoelectric and radiation $m = Nr = 0$, the amounts of temperature are 0.18355, 0.20745, and 0.23129. It is evidently seen that the increase in temperature is 0.08587 for the Eckert number 0.30, as there is both radiation and Hall current at $Y = 2.50627$. The Eckert number, which is crucial for system design and analysis when heat generation and transport are key elements, is better understood thanks to this result.

In Fig. 10, the combined impacts of thermoelectric and radiation have been shown for non-Newtonian (Casson) fluid as well as Newtonian fluid. If we observe a little better, we can see that the temperature outlines are enhanced by the rise in the value of the Hall effect and radiation combined for both fluids. But the value of temperature for non-

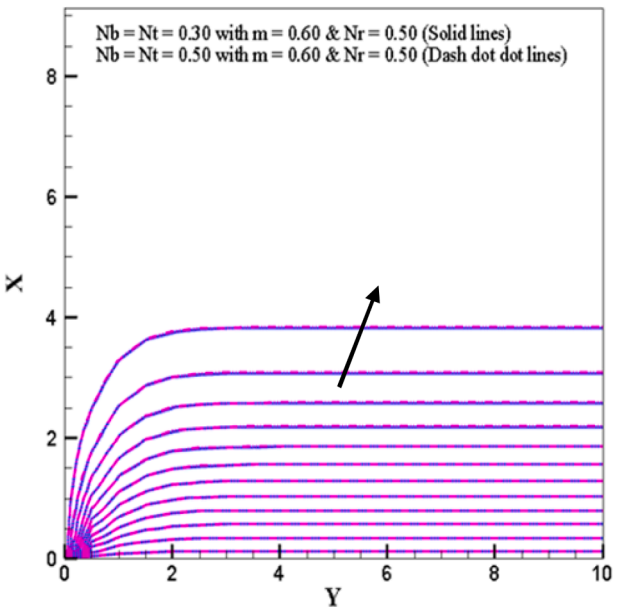

Fig. 21. Stream lines for changing N_b and N_t with presence of N_r and m.

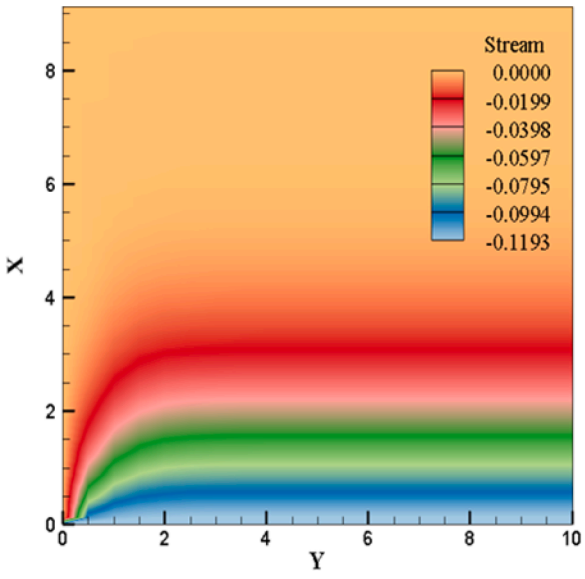

Fig. 22. Flood representation of Fig. 21.

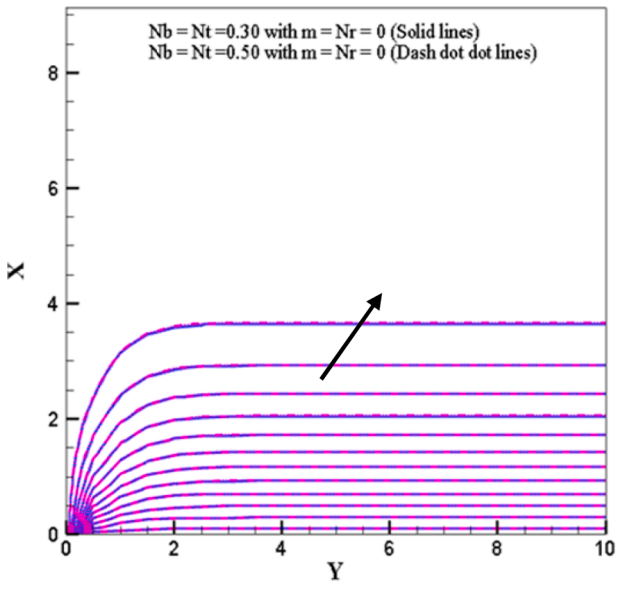

Fig. 23. Streamlines for changing N_b and N_t with the absence of N_r and m.

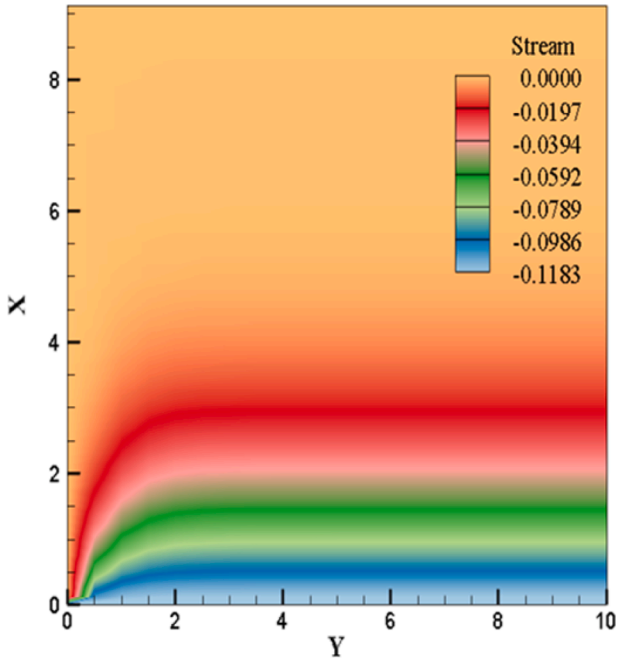

Fig. 24. Flood display of Fig. 23.

Newtonian (Casson) fluid is comparatively high compared to Newtonian fluid. This outcome demonstrates a considerable correlation between the effects of radiation and Hall current individually and the prior article [29,50,51].

The impression of Lewis number *Le* on concentration profiles has been demonstrated in Fig. 11, and including an increment in Lewis number *Le*, it is revealed that the concentration profiles reduce for both fluids (Newtonian and non-Newtonian fluids). A closer look reveals that the value of concentration for Newtonian fluid is a little higher compared to non-Newtonian (Casson) fluid under $Y < 2.25032$.

From Fig. 12, it can be remarked that the deviation of concentration profiles with respect to the thermophoresis parameter is against the Y direction, and it can also be seen that the concentration outlines upturns because of the increasing value of the thermophoresis parameter for both fluids. But the values of concentration for Newtonian fluid are slightly higher than those for non-Newtonian (Casson) fluid at the boundary layer. The cumulative consequences of radiation and thermoelectricity on the stream lines and advanced visualisation for both fluids are shown in Figs. 13–16. The profile of the stream line for non-Newtonian (Casson) fluid is described in Fig. 13, and it is detected that the stream lines are comparatively higher than the Newtonian fluid, which is shown in Fig. 15. Fig. 14 deals with the advanced look of Figs. 13, and 16 is for Fig. 15.

For both fluids, the mutual impact of thermoelectric as well as radiation on the isothermal lines and advanced visualisation are shown in Figs. 17–20. In Fig. 17, the shape of the isothermal line for non-Newtonian (Casson) fluid is depicted, and it can be seen that the isothermal lines are relatively higher than those for Newtonian fluid, as shown in Fig. 19. Fig. 18 depicts a more sophisticated version of Fig. 17, whereas Fig. 20 depicts Fig. 19.

The dominance of the Brownian parameter and thermophoresis parameter on streaming lines and adiabatic lines has been exhibited in

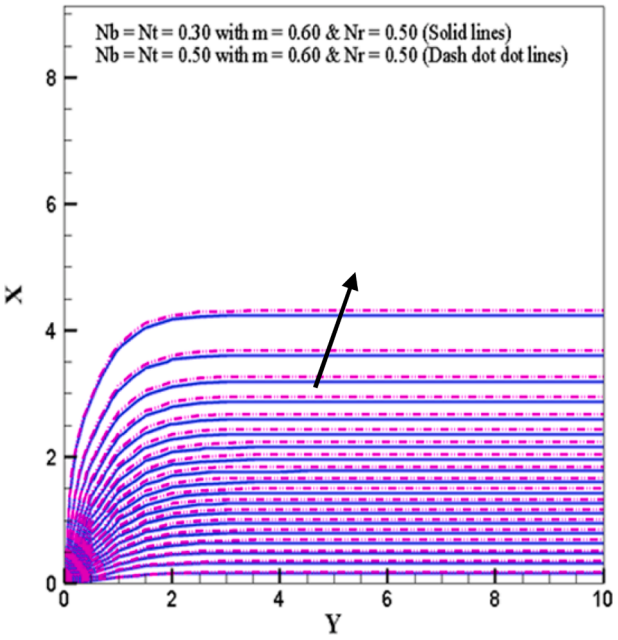

Fig. 25. Isothermal lines for changing N_b and N_t with the presence of N_r and m.

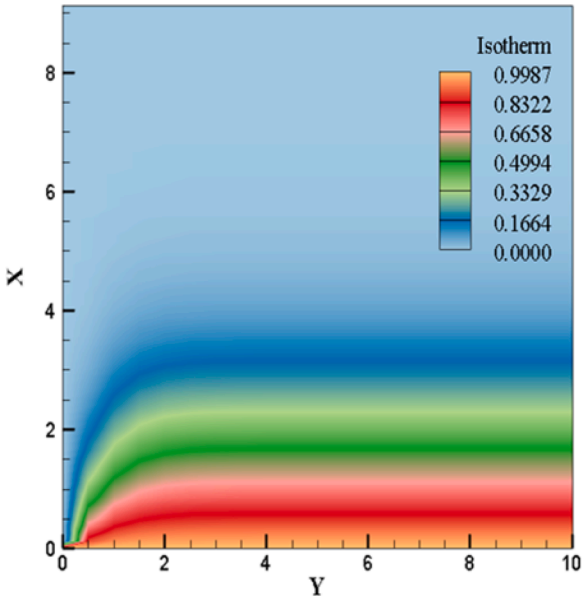

Fig. 26. Flood visualize of Fig. 25.

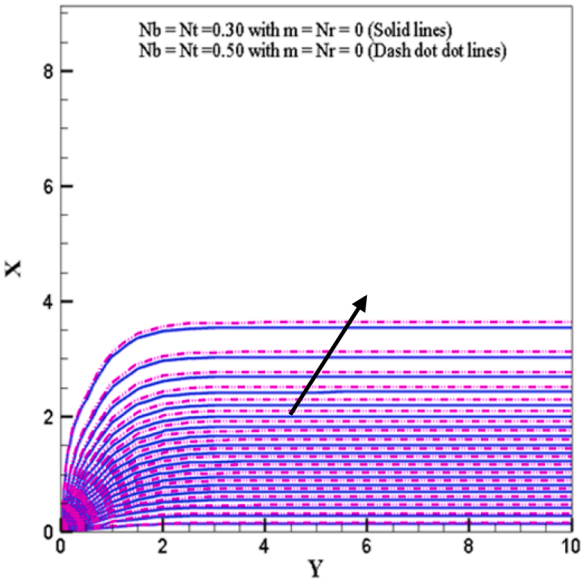

Fig. 27. Isothermal lines for changing N_b and N_t with absence of N_r and m.

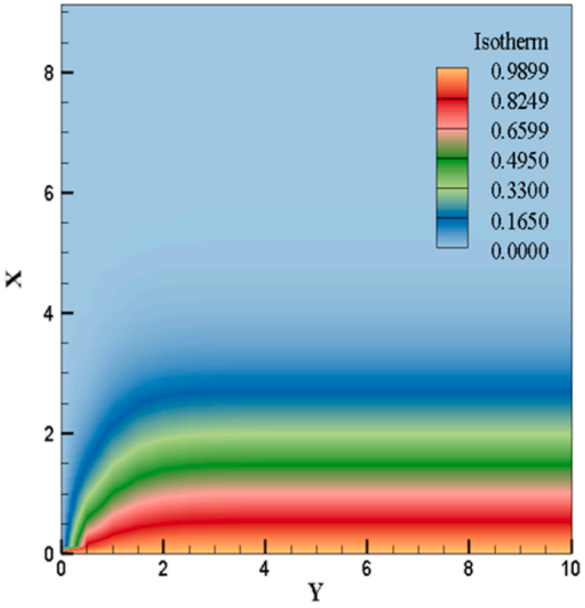

Fig. 28. Flood perspective of Fig. 27.

Figs. 21–28. From Fig. 21 to Fig. 24, the streamlines and isothermal lines have been figured out with the omission of thermoelectric and thermal radiation, but Figs. 25 to Fig. 28 have been drawn with the existence of thermal radiation as well as thermoelectric. It is evident that the isotherms and streamlines are more relevant when Hall current and radiation are present, implying that the isotherms and streamlines in the presence of those parameters are more significant than when they are absent.

Fig. 29 represents the combined impressions of thermal radiation and thermoelectric on the skin friction for both fluids, such as Newtonian fluids and non-Newtonian fluids, and with improvements in thermoelectric and thermal radiation values, it is noted that skin friction for both fluids drops., but if we compare with respect to fluid and it is observed that the amount of skin friction of Newtonian fluid is relatively high from non-Newtonian fluid. Fig. 30 explores the consequences of the Grashof number on skin friction for both Newtonian as well as non-Newtonian fluids. It is noticeable that skin friction declines as the Grashof number increases slightly, but when comparing fluids, it is evident that the amount of skin friction for Newtonian fluid is relatively high compared to non-Newtonian fluid (Casson).

The relation between the Nusselt number and Joule number for both Newtonian and non-Newtonian fluids is examined in Fig. 31. Convective heat transfer is characterised by the Nusselt number, whereas Joule heating via electric currents is characterised by the Joule number. For both fluid types, it is discovered that Nusselt numbers fall as Joule numbers climb. For heat transfer to occur in electrically conductive fluids, this inverse correlation is essential. The thermal driving power for convective heat transmission is decreased by joule heating, which boosts fluid temperatures close to conducting materials. These discoveries have important ramifications for electrically conductive fluid applications, including electronic cooling and chemical reactors.

In Fig. 32, it is shown how the Sherwood number in both Newtonian

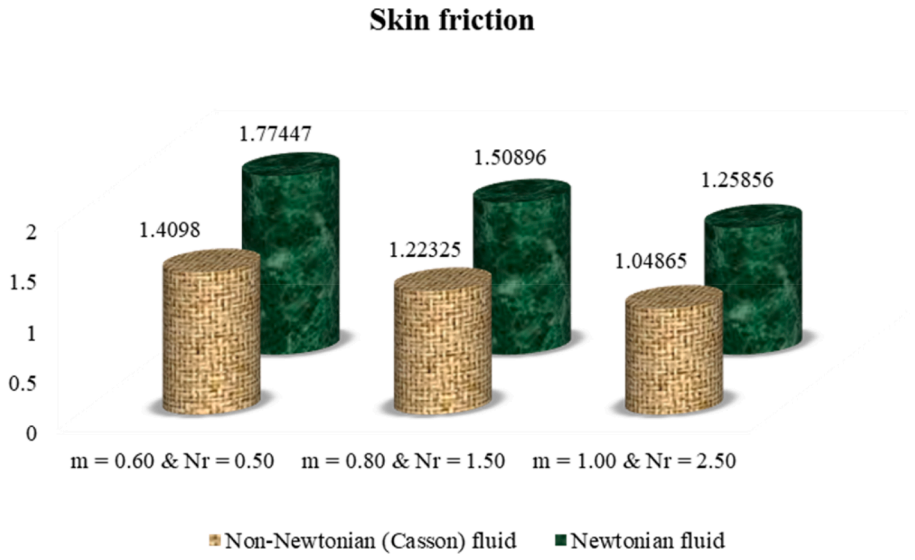

Fig. 29. Model of skin friction generated by impacts of radiation and thermoelectric, jointly.

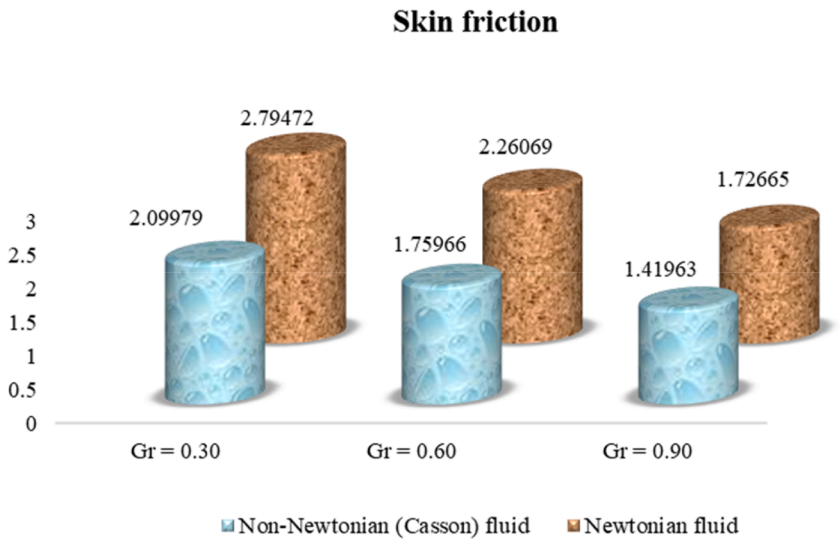

Fig. 30. Impacts of Grashof number *Gr* on skin friction.

and non-Newtonian fluids is impacted by radiation and Hall current factors. Sherwood numbers rise in both fluid types simultaneously when the radiation and Hall current parameters are increased. This dimensionless number, which is impacted by radiation and Hall currents, describes mass transfer rates. Mass transfer rates are greatly increased when these parameters are increased, especially for non-Newtonian fluids. Because they differ from Newtonian fluids in their unique rheological characteristics, non-Newtonian fluids exhibit a more prominent reaction Fig. 1.

8. Validation of results

To confirm the veracity of the research's conclusions, a table and a bar graph are displayed in Table 2 and Fig. 33, respectively. Both the table and figure display a high level of consistency with the findings of the most recent studies, which have been performed by Ali et al. [29] and Reza-E-Rabbi et al. [30].

9. Conclusions

Unsteady 2D Casson nanofluid of magnetohydrodynamics flow on a stretchable sheet with the combination of radiant energy and Hall current has been studied in this investigation. The combined impression of these parameters have improved the indicated fluid fileds significantly rather than their individual influences. Moreover, It is observed that the physical phenomena of Newtonian fluid flow did not grow as much as non-Newtonian (Casson) fluid for most of the parameters. A finite difference scheme has been employed to numerically solve the system of dimensionless PDEs with their associated boundary conditions. The numerical outcomes gained in this work comprise the impression of different parameters. The key outcomes are:

- The primary velocity profiles U improve due to the growth of the thermophoresis factor N_t and the combined increases of the radiation parameter N_r and Hall current parameter m for both fluids (Newtonian fluid as well as Casson fluid), though the velocity is comparatively lower for the Newtonian fluid flow than the Casson fluid. On

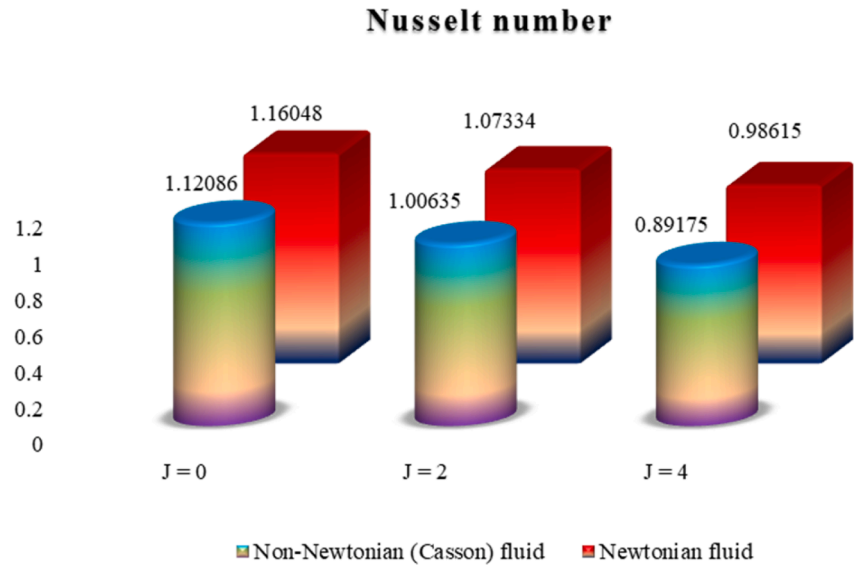

Fig. 31. Nusselt number model with the impacts of Joule number.

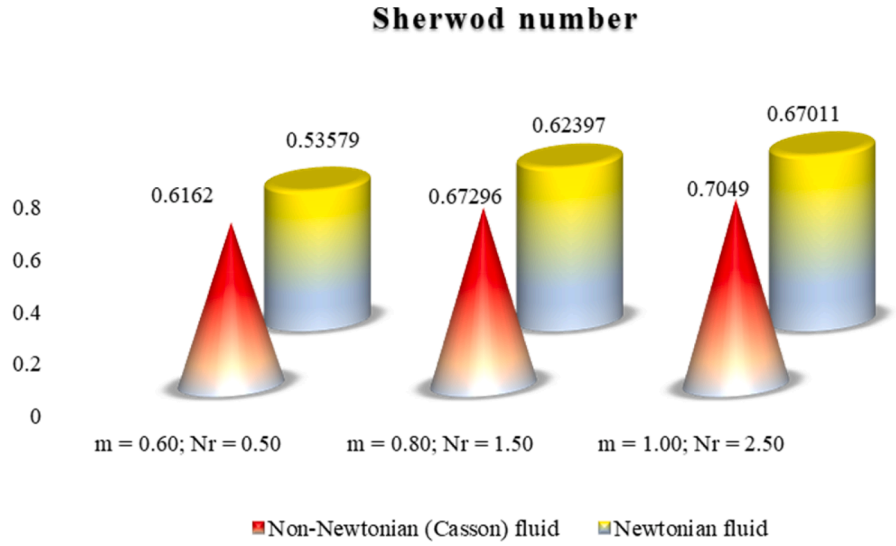

Fig. 32. Sherwood number model from combined radiation and thermoelectric effects.

Table 2
Validation with previous results.

Increased parameters	Earlier outcomes provided by								Current study			
	Reza-E-Rabbi et al. [30]				Ali et al. [29]							
	U	W	T	C	U	W	T	C	U	W	T	C
M	D				D	I			D	I		
M					I	I			I	I		
N_r			I		I		I		I		I	
Le				D				D				D
Γ	D								D			

* I for increase; D for decrease.

the other hand, the primary velocity profiles U decrease due to a rise in magnetic parameter M and Casson parameter γ.

- The secondary velocity profiles for both fluids (Newtonian fluid as well as Casson fluid) grow with an increase in the thermophoresis parameter N_t and the magnetic parameter M, albeit the Casson fluid's velocity is comparably lower than Newtonian fluid's in the boundary layer area.
- The improvement of the temperature profiles T is caused by an increase in the Eckert number Ec and a simultaneous rise in the radiation parameter N_r and Hall current parameter m.

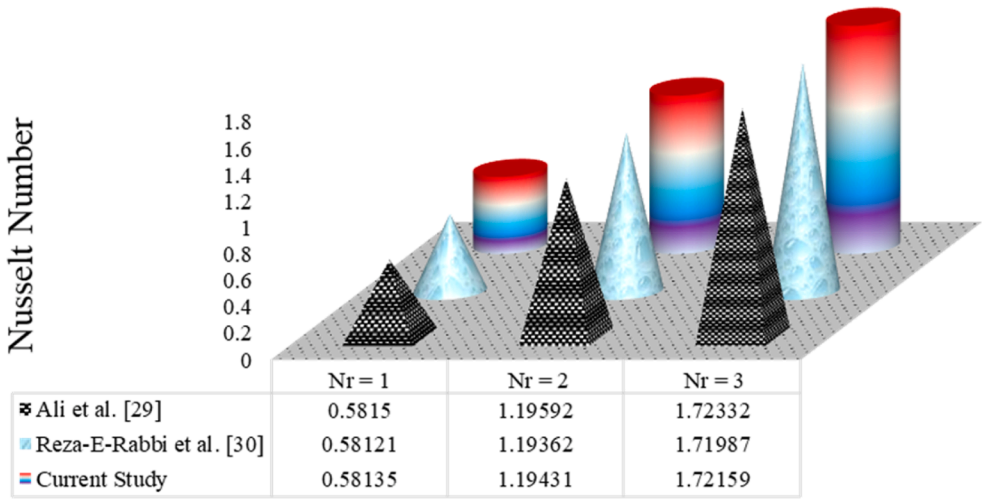

	Nr = 1	Nr = 2	Nr = 3
Ali et al. [29]	0.5815	1.19592	1.72332
Reza-E-Rabbi et al. [30]	0.58121	1.19362	1.71987
Current Study	0.58135	1.19431	1.72159

Fig. 33. Validation schematic in contrast to prior studies.

- Concentration profiles C decrease with increasing the Lewis number Le, while they increase with increasing the thermophoresis parameter N_t.
- With an increase in radiation parameters N_r and Hall current m simultaneously, for both fluid flows, the local skin friction decreases and the Grashof number improves, although the skin friction of Newtonian fluid is greater than that of Casson fluid, whereas the isothermal and stream lines progressively grow.
- Both Newtonian and non-Newtonian fluids experience a drop in the Nusselt number when the Joule number rises. Additionally, it emphasis how Newtonian fluids at equal Joule number values have better heat transport capabilities than non-Newtonian fluids.
- Non-Newtonian fluids have a more strong reaction, and the Sherwood number rises with increasing radiation and thermoelectric parameter values.

This conceptual research can be potentially applied to various non-Newtonian fluids, such as Bingham fluids, Maxwell fluids, or dilatant fluids. It encompasses phenomena like periodic magnetohydrodynamics (MHD), quadratic convection, non-linear radiation, exponential heat sources, and more. Furthermore, this research can be expanded by introducing electric fields into the study, specifically in the context of second-grade and third-grade fluids.

Declaration of Competing Interest

The authors declare that they have no known competing financial interests or personal relationships that could have appeared to influence the work reported in this paper.

Data availability

The data that has been used is confidential.

Acknowledgements

Qatar National Library provided funding for the publishing of this article.

References

[1] S.U.S. Choi, Enhancing thermal conductivity of fluids with nanoparticles, ASME Int. Mech. Eng. 66 (1995) 99–105.
[2] N. Casson, A flow equation for pigment oil suspensions of the printing ink type, Open J. Fluid Dyn. 6 (4) (1959) 84–102.
[3] M. Abd El-Aziz, A.A. Afify, Effect of Hall current on MHD slip flow of Casson nano-fluid over a stretching sheet with zero nanoparticle mass flux, Thermophys. Aeromech. 26 (3) (2019) 429–443.
[4] W. Jamshed, S. Uma Devi, M. Goodarzi, M. Prakash, K.S. Nisar, M. Zakarya, A. H. Abdel-Aty, Evaluating the unsteady Casson nano-fluid over a stretching sheet with solar thermal radiation: an optimal case study, Case Stud. Therm. Eng. 26 (2021), 101160.
[5] A. Kumar, R. Tripathi, R. Singh, M.A. Sheremet, Entropy generation on double diffusive MHD Casson nano-fluid flow with convective heat transfer and activation energy, Ind. J. Phys. 95 (2020) 1423–1436.
[6] K.B. Siddiqui, S. Batool, M.Y. Malik, M.Q. Hassan, A.S. Alqahtani, Darcy Forchheimer bioconvection flow of Casson nano-fluid due to a rotating and stretching disk together with thermal radiation and entropy generation, Case Stud. Therm. Eng. 27 (2021), 101201.
[7] A. Sahoo, R. Nandkeolyar, Entropy generation in convective radiative flow of a Casson nano-fluid in non-Darcy porous medium with Hall current and activation energy: the multiple regression model, Appl. Math. Comput. 402 (2021), 125923.
[8] S.M. Abo-Dahab, M.A. Abdelhafez, F. Mebarek-Oudina, S.M. Bilal, MHD Casson nano-fluid flow over nonlinearly heated porous medium in presence of extending surface effect with suction/injection, Ind. J. Phys. (2021) 1–15.
[9] G.R. Ganesh, W. Sridhar, MHD radiative Casson—nano-fluid stream above a nonlinear extending surface including chemical reaction through Darcy-Forchiemer medium, Heat Transf. 50 (8) (2021) 7691–7711.
[10] F. Ahmad, S. Abdal, H. Ayed, S. Hussain, S. Salim, A.O. Almatroud, The improved thermal efficiency of Maxwell hybrid nano-fluid comprising of graphene oxide plus silver /kerosene oil over stretching sheet, Case Stud. Therm. Eng. 27 (2021), 101257.
[11] S. Reza-E-Rabbi, S.M. Arifuzzaman, T. Sarkar, M.S. Khan, S.F. Ahmmed, Explicit finite difference analysis of an unsteady MHD flow of a chemically reacting Casson fluid past a stretching sheet with Brownian motion and thermophoresis effects, J. King Saud Univ. Sci. 32 (1) (2020) 690–701.
[12] A.T. Akinshilo, F. Mabood, A.O. Ilegbusi, Heat generation and nonlinear radiation effects on MHD Casson nano-fluids over a thin needle embedded in porous medium, Int. Commun. Heat Mass Transf. 127 (2021), 105547.
[13] S. Nadeem, B. Ishtiaq, M.B.B. Hamida, S. Almutairi, H.A. Ghazwani, S.M. Eldin, A. S. Al-Shafay, Reynolds nano fluid model for Casson fluid flow conveying exponential nanoparticles through a slandering sheet, Sci. Rep. 13 (1) (2023) 1953.
[14] A.H. Majeed, R. Mahmood, H. Shahzad, A.A. Pasha, Z.A. Raizah, H.A. Hosham, D.S. K. Reddy, M.B. Hafeez, Heat and mass transfer characteristic in MHD Casson fluid flow over a cylinder in a wavy channel: higher-order FEM computations, Case Stud. Therm. Eng. 42 (2023), 102730.
[15] M. Shoaib, M. Kausar, K.S. Nisar, M.A.Z. Raja, A. Morsy, Impacts of thermal energy on MHD Casson fluid through a Forchheimer poros medium with inclined non-linear surface: a soft computing approach, Alex. Eng. J. 61 (2022) 12211–12228.
[16] H. Waqas, U. Farooq, R. Naseem, S. Hussain, M. Alghamdi, Impact of MHD radiative flow of hybrid nano-fluid over a rotating disk, Case Stud. Therm. Eng 26 (2021), 101015.
[17] A.B. Patil, P.P. Humane, V.S. Patil, G.R. Rajput, MHD Prandtl nano-fluid flow due to convectively heated stretching sheet below the control of chemical reaction with thermal radiation, Int. J. Ambient Energy. (2021) 1–13.
[18] S.E. Ghasemi, S. Mohsenian, S. Gouran, A. Zolfagharian, A novel spectral relaxation approach for nano-fluid flow past a stretching surface in presence of magnetic field and nonlinear radiation, Results Phys. 32 (2022), 105141.
[19] S.Z. Alamri, R. Ellahi, N. Shehzad, A. Zeeshan, Convective radiative plane Poiseuille flow of nano-fluid through porous medium with slip: an application of Stefan blowing, J. Mol. Liq. 273 (2019) 292–304.
[20] j. Yin, X. Zhang, M.I.U. Rehman, A. Hamid, Thermal radiation aspect of biconvection flow of magnetized Sisko nano-fluid along a stretching cylinder with swimming microorganisms, Case Stud. Therm. Eng. 30 (2022), 101771.

[21] R. Mahat, M. Saqib, I. Khan, S. Shafie, N.A.M. Noor, Thermal radiation effect on viscoelastic Walters'-B nano-fluid flow through a circular cylinder in convective and constant heat flux, Case Stud. Therm. Eng. 39 (2022), 102394.
[22] S.M.R.S. Naqvi, H. Waqas, S. Yasmin, D. Liu, T. Muhammad, S.M. Eldin, S.A. Khan, Numerical simulations of hybrid nano-fluid flow with thermal radiation and entropy generation effects, Case Stud. Therm. Eng. 40 (2022), 102479.
[23] U. Farooq, H. Waqas, R. Makki, M.R. Ali, A. Alhushaybari, T. Muhammad, M. Imran, Computation of Cattaneo-Christov heat and mass flux model in Williamson nano-fluid flow with biconvection and thermal radiation through a vertical slender cylinder, Case Stud. Therm. Eng. 42 (2023), 102736.
[24] N. Tarakaramu, P.V.S. Narayana, N. Sivakumar, D.H. Babu, K.B. Lakshmi, Convective conditions on 3D magnetohydrodynamics (MHD) non-Newtonian nano-fluid flow with nonlinear thermal radiation and heat absorption: a numerical analysis, J. Nanofluids 12 (2023) 448–457.
[25] A. Saeed, M. Jawad, W. Alghamdi, S. Nasir, T. Gul, P. Kumam, Hybrid nano-fluid flow through a spinning Darcy-Forchheimer porous space with thermal radiation, Sci. Rep. 11 (2021) 16708.
[26] M.Z. Swalmeh, F.A. Alwawi, M.S. Kausar, M.A.H. Ibrahim, A.S. Hamarsheh, I. M. Sulaiman, A.M. Awwal, N. Pakkaranang, B. Panyanak, Numerical simulation on energy transfer enhancement of a Williamson ferrofluid subjected to thermal radiation and a magnetic field using hybrid ultrafine particles, Sci. Rep. 13 (2023) 3176.
[27] J. Wang, W.A. Khan, Z. Asghar, M. Waqas, M. Ali, M. Irfan, Entropy optimized stretching flow based on non-Newtonian radiative nanoliquid under binary chemical reaction, Comput. Methods Prog. Biomed. 188 (2020), 105274.
[28] A. Ganjikunta, H.B. Kommaddi, V. Bhajanthri, R. Kodi, An unsteady MHD flow of a second-grade fluid passing through a porous medium in the presence of radiation absorption exhibits Hall and ion slip effects, Heat Transf. 52 (1) (2023) 780–806.
[29] M.Y. Ali, S. Reza-E-Rabbi, M.M.H. Rasel, S.F. Ahmmed, Combined impacts of thermoelectric and radiation on hydromagnetic nano-fluid flow over a nonlinear stretching sheet, Partial Differ. Equ. App. Math. 7 (2023), 100500.
[30] S. Reza-E-Rabbi, S.F. Ahmmed, S. Islam, S.M. Arifuzzaman, B.M.J. Rana, M.Y. Ali, M.S. Khan, Characterization of fluid flow and heat transfer of a periodic magnetohydrodynamics nano non-Newtonian liquid with Arrhenius activation energy and nonlinear radiation, Heat Transf. 51 (2022) 6578–6615.
[31] S. Reza-E-Rabbi, M.Y. Ali, S.M. Arifuzzaman, M.S. Khan, S.F. Ahmmed, Numerical modelling of a non-linear radiative non-newtonian nano-fluid flow with arrhenius activation energy, KU Stud. Special Issue (ICSTEM4IR): (2022) 291–306.
[32] M.Y. Ali, S. Reza-E-Rabbi, S.F. Ahmmed, Radiation and hall current impressions on Newtonian and Bingham fluids flow past a stretching surface, KU Stud. Special Issue (ICSTEM4IR): (2022) 307–320.
[33] M.D. Shamshuddin, N. Akkurt, A. Saeed, M.D. Kumam, Radiation mechanism on dissipative ternary hybrid nano-fluid flow through rotating disk encountered by Hall currents: HAM solution, Alex. Eng. J. 65 (2023) 543–559.
[34] P. Li, A. Abbasi, E.R. El-Zahar, W. Farooq, Z. Hussain, S.U. Khan, M.I. Khan, S. Farooq, M.Y. Malik, F. Wang, Hall effects and viscous dissipation applications in peristaltic transport of Jeffrey nano-fluid due to wave frame, Colloids Interface Sci. Commun. 47 (2022), 100593.
[35] M. Khan, W. Ali, J. Ahmed, A hybrid approach to study the influence of Hall current in radiative nano-fluid flow over a rotating disk, Appl. Nanosci. 10 (12) (2020) 5167–5177.
[36] S.M. Hussain, J. Jain, G.S. Seth, M.M. Rashidi, Free convective heat transfer with Hall effects, heat absorption and chemical reaction over an accelerated moving plate in a rotating system, J. Magn. Magn. Mater. 422 (2017) 112–123.
[37] A. Khan, W. Kumam, I. Khan, A. Saeed, T. Gul, P. Kumam, I. Ali, Chemically reactive nano-fluid flow past a thin moving needle with viscous dissipation, magnetic effects and hall current, PLoS ONE 16 (4) (2021), e0249264.
[38] S.A. Khan, T. Hayat, A. Alsaedi, Irreversibility analysis in Darcy-Forchheimer flow of viscous fluid with Dufour and Soret effects via finite difference method, Case Stud. Therm. Eng. 26 (2021), 101065.
[39] M. Venkateswarlu, G.V.R. Reddy, D.V. Lakshmi, Unsteady MHD flow of a viscous fluid past a vertical porous plate under oscillatory suction velocity, Adv. Appl. Sci. Res. 4 (6) (2013) 52–67.
[40] B. Ali, S. Hussain, Y. Nie, A.K. Hussein, D. Habib, Finite element investigation of Dufour and Soret impacts on MHD rotating flow of Oldroyd-B nano-fluid over a stretching sheet with double diffusion Cattaneo Christov heat flux model, Powder Technol. 377 (2020) 439–452.
[41] Z. Uddin, K.S. Vishwak, S. Harmand, Numerical duality of MHD stagnation point flow and heat transfer of nano-fluid past a shrinking/stretching sheet: metaheuristic approach, Chin. J. Phys. 73 (2021) 442–461.
[42] N. Kakar, A. Khalid, A.S. Al-Johani, N. Alshammari, I. Khan, Melting heat transfer of a magnetized water-based hybrid nano-fluid flow past over a stretching/shrinking wedge, Case Stud. Therm. Eng. 30 (2022), 101674.
[43] D. Gopal, S. Jagadha, P. Sreehari, N. Kishan, D. Mahendar, A numerical study of viscous dissipation with first order chemical reaction and ohmic effects on MHD nano-fluid flow through an exponential stretching sheet, Mater. Today: Proc. 59 (2022) 1028–1033.
[44] S. Reza-E-Rabbi, S.F. Ahmmed, S.M. Arifuzaman, T. Sarkar, M.S. Khan, Computational modelling of multiphase fluid flow behaviour over a stretching sheet in the presence of nanoparticles, Eng. Sci. Technol. Int. J. 23 (3) (2020) 605–617.
[45] S.M. Arifuzzaman, M.S. Khan, A. Al-Mamun, S. Reza-E-Rabbi, P. Biswas, I. Karim, Hydrodynamic stability and heat and mass transfer flow analysis of MHD radiative fourth-grade fluid through porous plate with chemical reaction, J. King Saud Univ. Sci. 31 (4) (2019) 1388–1398.
[46] M.M. Bhatti, E.E. Michaelides, Study of Arrhenius activation energy on the thermo-bioconvection nano-fluid flow over a Riga plate, J. Therm. Anal. Calorim. 143 (2021) 2029–2038.
[47] L.M. Iva, M.S. Hasan, S.K. Paul, R.N. Mondal, MHD free convection heat and mass transfer flow over a vertical porous plate in a rotating system with Hall current, heat source and suction, Int. J. Adv. Appl. Math. Mech. 6 (1) (2018) 49–64.
[48] A.H. Pordanjani, A. Raisi, B. Ghasemi, Numerical simulation of the magnetic field and Joule heating effects on force convection flow through parallel-plate microchannel in the presence of viscous dissipation effect, Numer. Heat Transf., Part A: Appl. 76 (6) (2019) 499–516.
[49] A. Mushtaq, M. Mustafa, T. Hayat, A. Alsaedi, Nonlinear radiative heat transfer in the flow of nanofluid due to solar energy: a numerical study, J. Taiwan Inst. Chem. Eng. 45 (4) (2014) 1176–1183.
[50] H.U. Rasheed, S. Islam, W.Khan Zeeshan, J. Khan, T. Abbas, Numerical modeling of unsteady MHD flow of Casson fluid in a vertical surface with chemical reaction and Hall current, Adv. Mech. Eng. 14 (3) (2022), 16878132221085429.
[51] C. Sulochana, M. Poornima, Unsteady MHD Casson fluid flow through vertical plate in the presence of Hall current, SN Appl. Sci. 1 (2019) 1–14.
[52] A.A. Opanuga, S.O. Adesanya, H.I. Okagbue, O.O. Agboola, Impact of Hall current on the entropy generation of radiative MHD mixed convection casson fluid, Int. J. Appl. Comput. Math. 6 (2020) 1–18.